March 2018

The Stability of Sand Waves in a Tidally-Influenced Shipping Channel, Tampa Bay, Florida

John Willis Gray
University of South Florida, jwg1229@gmail.com

The Stability of Sand Waves in a Tidally-Influenced Shipping Channel, Tampa Bay, Florida

by

John Willis Gray

A thesis submitted in partial fulfillment
of the requirements for the degree of
Master of Science
with a concentration in Geological Oceanography
College of Marine Science
University of South Florida

Major Professor: David F. Naar, Ph.D.
Gregg R. Brooks, Ph.D.
Carl T. Friedrichs, Ph.D.
Mark E. Luther, Ph.D.

Date of Approval
May 23, 2018

Keywords: multibeam, bathymetry, backscatter, sediment, bedforms, ADCP, Sunshine Skyway Bridge

ACKNOWLEDGMENTS

I would like to first thank my committee members, Dr. David Naar, Dr. Gregg Brooks, Dr. Mark Luther, and Dr. Carl Friedrichs. I would also like to thank the Florida Institute of Oceanography, especially Rob Walker and the captains and crews of the R/V *Weatherbird II* and the R/V *Bellows*. Thanks are also due to the Continental-Shelf Characterization, Assessment, and Mapping Project, for incorporating transits in the center of the channel beneath the Sunshine Skyway Bridge into each of their cruises. Funding for these cruises was provided by the National Fish and Wildlife Foundation though the Gulf Environmental Benefit Fund, Grant #45892. I am also grateful for the help of the University of South Florida Ocean Monitoring and Prediction Lab, as well as the Eckerd College Sedimentology Lab. Special thanks are due to Jesse Hoemann and Ian Dow for their expertise and support. Last but not least, I would like to thank my wife, labmate, and colleague, Jennifer Brizzolara, for her support in every way for the duration of this project and my time in graduate school.

TABLE OF CONTENTS

LIST OF TABLES

LIST OF FIGURES

ABSTRACT

Tidally-influenced sandwaves are common coastal features present in various settings, including shipping channels. The main shipping channel in Tampa Bay under the Bob Graham Sunshine Skyway Bridge (a.k.a. the Skyway Bridge) contains such sandwave bedforms. Between the years 2000 and 2017, these bedforms have been surveyed with multibeam echosounders (MBES) on 21 occasions with ranging coverage and quality of returns. Surveys between 2000 and 2009 used a 300 kHz Kongsberg EM3000; surveys between 2015 and 2017 used a 400 kHz Reson Seabat 7125. For comparable surveys, bathymetry, backscatter, slope, curvature, planform curvature, and profile curvature maps were created and analyzed. Spectral analyses were completed on the same cross-section for usable surveys, providing a period and amplitude for the bedforms. Sediment samples were taken in September 2015 using a Shipek grab. The sediment samples were analyzed for grain size and carbonate content. A bottom-mounted ADCP recorded velocity data semi-continuously over the same time period. These data were analyzed in an effort to investigate the forcing mechanisms that influence the bedform morphology.

Mean grain sizes in the shipping channel under the Skyway Bridge range from 0.01 φ (0.99 mm, coarse sand) to 1.55 φ (0.34 mm, medium sand). Calcium carbonate content ranges from 25% to 87%. The sediment sample site most representative of the sandwave bedforms has a mean grain size of 0.01 φ and a calcium carbonate content of 87%. The calculated mean current velocity required to initiate transport of the D_{50} and D_{84} grain size percentile of the representative sediment sample site is 0.70 m/s and 1.05 m/s, respectively. Analysis of the ADCP-recorded velocity data shows that the calculated D_{50} critical velocity is frequently reached by peak flood and peak ebb currents except during neap tides, while the D_{84} critical velocity is reached only intermittently, mostly during spring tides. Analysis of MBES backscatter shows similar spatial patterns in two larger MBES surveys in 2004 and 2015. Bathymetric analysis of the sandwaves shows consistent characteristics through time. Wave crest analysis reveals that

bedforms migrate in both the ebb and flood directions. Spectral analysis shows primary wave spatial frequencies range from 0.13 m^{-1} to 0.22 m^{-1}, and primary wave periods range from 4.5 m to 6.0 m. The predominant wavelength of sandwaves within the study area is about 5 m, with an average wave height of 0.47 m. The maximum wave height along the axial cross-section analyzed is 0.8 m, observed in April 2017.

The sediments comprising the sandwave bedforms are likely winnowed by tidal currents resulting in larger grain size and carbonate content than other areas of the shipping channel and surrounding bay. Consistent patterns in MBES backscatter over time indicate that the sediment distribution pattern in the study area have not significantly changed. The size and shape of the bedforms in the shipping channel beneath the Skyway Bridge are have been in a quasi-dynamic equilibrium over the past 13 years. The bedforms are shown to migrate in both the ebb and flood directions despite an average faster ebb current velocity than a flood current velocity. More frequent and consistent MBES surveys as well as more continuous ADCP data availability would allow for better understanding of sediment transport via bedform migration in tidally-influenced environments.

1. INTRODUCTION, BACKGROUND, AND STUDY AREA

1.1 Introduction

Sand wave bedforms persist within the Tampa Bay shipping channel, including the narrow pass beneath the Bob Graham Sunshine Skyway Bridge, herein referred to as the Skyway Bridge. Sand waves are large, asymmetrical, flow-transverse, sub-aqueous bedforms (Bates and Jackson, 1984). These dynamic bedforms occur in a wide range of settings, sizes, and shapes. Settings include tidal sand banks, individual shoals, shoreface-connected ridges, and within channels (Knaapen and Hulscher, 2002; Stolk, 2000; Levin et al., 1992).

These bedforms are commonly found in high-velocity zones of tidally-influenced estuaries that have an available sand supply, including Tampa Bay. The Gironde Estuary in France contains sand waves at the entrance ranging from 1.5-6.7 m high, with wavelengths of 37-182 m (Berné et al., 1993). Adolphus Channel in the Torres Strait region of Australia has sand waves averaging 3.9 m high with wavelengths averaging 102 m (Harris, 1988). The Minas Basin and Cobequid Bay within the Bay of Fundy include intertidal sand waves with wave heights of 0.15–3.4 m and wavelengths of 5.2–215 m (Dalrymple, 1984). Giant sand waves on the ebb tidal delta at the entrance to San Fransisco Bay have a maximum height of 10 m and a maximum wavelength of 220 m (Barnard et al., 2006; Sterlini et al., 2009; Elias and Hansen, 2013).

Sand waves are also found within dredged channels. Crests of sand waves in the Jade shipping channel in North Germany create a hazard to navigation, as the crests of the sand waves become too shallow (Redding, 2000). The Bisanseto Channel in Japan contains stable sand waves that tend to reform after dredging (Knaapen and Hulscher, 2002; Katoh et al., 1999).

To investigate the morphology and dynamics of modern natural sand waves, a combination of sediment characteristics, flow velocities, and bathymetric data are used. Bathymetric data can be provided by subaqueous observations in the case of intertidal sand waves, using single-beam sonar, side-scan sonar, and multibeam echosounders (MBES). Sediment characteristics must be determined from analysis of sediment samples. Flow velocities can be determined utilizing acoustic Doppler current profilers (ADCP) that measure current velocities throughout the water column.

Modeling sand waves in a controlled environment, such as a flume, can help to determine the relationships between current velocities, sediment character, and sand wave formation and migration (De Visser, 1997; Rubin and McCulloch, 1980; Yalin, 1964). Modeling of naturally occurring sand waves requires precise boundary conditions. A long-term time series of high resolution data can contribute to the effort understanding sand wave bedform dynamics (van den Berg et al., 2012; van Santen et al., 2011). This investigation will treat the Skyway channel as a natural laboratory to measure, monitor, and analyze bedform characteristics.

1.2 Background

Tampa Bay, located on the gulf coast of Florida, is a Y-Shaped estuary (Figure 1). It is the largest Florida estuary by area. The bay covers an area of 5,700 km^2 and has an average depth of 3.7 m (Goodell and Gorsline, 1961). The water level and currents of Tampa Bay are primarily controlled by tides and weather effects. Beneath the Skyway Bridge, which crosses the mouth of Tampa Bay, currents are 95% attributed to tides (Weisberg and Zheng, 2006). The surface sediments of Tampa Bay are predominantly comprised of siliciclastics with varying amounts of carbonate clastics (Doyle et al., 1989). These surface sediments can be divided into three zones: clastic muds can be found in the upper bay and land-bay interface around the bay, siliciclastic sands dominate the open portion of the middle bay, and carbonate sands and gravels are found in the lower bay (Brooks and Doyle, 1998).

Tampa Bay's morphology has been modified for various societal needs between 1880 and the present time (Goodwin, 1987). These anthropomorphic features include ship channels, dredge spoil

disposal sites, spoil islands, bridges and causeways, residential and commercial landfills, maintained inlets, and nourished beaches. These types of features affect the tidal prism and flow and, as a result, the underlying bedform morphology. The largest of these features is the main ship channel that passes under the Skyway Bridge. This main ship channel is the gateway to three ports (The Port of Tampa, Port Manatee and The Port of Saint Petersburg) from the Gulf of Mexico. The Port of Tampa currently ranks first in Florida and 19th in total trade by cargo volume of United States ports. The Port of Manatee ranks 6th in Florida and 90th in the United States. All three ports make Tampa Bay rank 17th in the United States (AAPA, 2016).

The heavily trafficked main ship channel of Tampa Bay was created, and is maintained, by the U.S. Army Corps of Engineers by dredging to a projected depth of 13 m (Figure 2). This dredged channel has been widened on multiple occasions including a project that was competed in 1985 (Goodwin, 1987) and a current project estimated to be competed in 2018 (Jackson and Parker, 2017). Port pilots navigate an assortment of large ships into and out of the ports of Tampa Bay including navigating under the Skyway Bridge. To safely accomplish this task, the pilots rely on the Physical Oceanographic Real-Time System (PORTS) that measures important navigational parameters such as water levels, water temperature, currents, salinity, winds, atmospheric pressure, and air temperature at a variety of locations though out Tampa Bay (NOAA, 2013). These data are provided in real-time to the pilots and archived.

1.3 Study Area and Data

The study area was confined to the sand wave bedform field in the portion of the shipping channel that passes underneath the Skyway Bridge (Figure 3). Between the years of 1998 and 2009, 300 kHz multibeam echosounder (MBES) data were collected during transits of opportunity in and out of Tampa Bay. Every transit passed through the ship channel beneath the Skyway Bridge, both inbound and outbound. Due to the constricted nature of the channel between bridge structures, many of these surveys passed over the same area. Analysis Area 1 (a.k.a. Area 1), indicated by the yellow box in Figure 3, contains 14 such datasets from 2000 to 2009. In 2004, a 300 kHz MBES survey was completed beneath

the Skyway Bridge, revealing sand waves concentrated in the center of the channel. In September 2015, a 400 kHz MBES survey of the ship channel overlapping the 2004 survey area was executed (bathymetry shown in Figure 3), and four sediment samples were concurrently collected (sample sites shown in Figure 3). Between the years of 2015 and 2017, 400 kHz MBES transit data were also strategically and opportunistically collected down the center of the ship channel, where the 2004 and 2015 surveys show sand wave bedforms.

Area 1, indicated by the yellow box in Figure 3, is an area of 390 m^2 in which 21 bathymetric data sets, collected episodically from 2000 to 2017, overlap. Analysis Area 2 (a.k.a. Area 2), indicated by the red box in Figure 3 and all following figures, is a larger area of 3087 m^2 that has seven overlapping bathymetric data sets collected episodically from 2015 to 2017. The profile line defined as A to A', shown as a black line in Figure 3, is 78 m in length and runs down the center of the larger Area 2. An acoustic Doppler current profiler (ADCP) located within the study area has been collecting current velocity data from February 1999–present as part of the NOAA Physical Oceanographic Real-Time System (PORTS). These real-time data are archived and publicly available at the Currents Measurements Interface for the Study of Tides (C-MIST).

2. METHODS

2.1 Sediment Samples

2.1.1 Collection and Processing Methods

Four sediment samples were collected using a Shipek Grab device on September 9, 2015 aboard the R/V *Bellows*. Navigation was from a MarineStar enabled differential GPS and is estimated to be accurate to within a horizontal accuracy of 10 cm with 95% certainty. Four sample sites were selected based on both the October 2004 and the concurrent September 2015 multibeam surveys (Figure 3). Sample Site 3 was in the center channel to capture the sediment that composes the sand wave bedforms. Sample Site 2 was chosen because it is likely hard bottom. The location of the sample sites were marked from a shipboard GPS upon the grab hitting bottom. The GPS location of the samples were corrected for the horizontal offset between GPS antenna and the winch block based on the ships heading. Observationally, the Shipek grab bucket for Sample Sites 1, 3, and 4 was full with mixed clastics. The sample from site 2 was limited in volume with mixed clastics and organics.

Each sample was washed to remove salt content, dried in an oven at 40°C, and split by the cone and quartering method as in Lewis and McConchie (1994) and Krumbein and Pettijohn (1938) into eight subsamples with the exception of Sample Site 2, where sample size was limited to two subsamples. The subsamples for each sample site were divided equally for grainsize and carbonate fraction analyses. Carbonate fraction was determined by acid leaching method as in Milliman (1974). Grain size was determined by a combination of methods. Grain size finer than 4 ϕ was determined by pipette analyses as in Folks and Antle (1965). Grain sizes between 4 ϕ and -1.0 ϕ were determined by Gibbs' (1974) settling tube method. Grain size coarser than -1.0 ϕ were determined by Folks and Antle (1965) sieve method.

The results of each subsample within each sample site were averaged using the arithmetic mean. Statistics were calculated on each sample using the method of moments (Folk, 1965). One outlier was eliminated due to human/instrument error.

2.1.2 Critical Shear Stress Analyses Methods

Shear stress analyses was conducted for sediment Sample Site 3, which is most representative of Areas 1 and 2 that are also near the center of the channel and contain sand waves. To estimate a minimum current velocity required to initiate sediment transport of the sand wave sediment, the von Kármán-Prandtl equation, also known as the law of the wall, was applied using the D_{50} and D_{84} grain size values measured from Sample Site 3 (Figures 4 and 5).

$$\frac{U}{\mu_*} = \left(\frac{1}{\kappa}\ln(\frac{y}{y_0})\right)$$

U is the mean fluid velocity needed to initiate transport of a grain of size D

μ_* is the shear velocity.

κ is von Karman's constant, generally set to 0.4 (Biron et al., 1998).

y is height above the boundary surface where the mean flow velocity U is reached, estimated as 0.4 multiplied by depth. y_0 is the height above the bed where mean flow is zero. The rough flow approximation is used y_0=3.5D/30. (Einstein and El-Samni, 1949; Kironoto and Graf, 1995; Afzalimehr and Rennie, 2009).

$$\mu_* = \sqrt{\frac{\tau_0}{\rho}}$$

τ_0 is the boundary shear stress (shear force applied to unit area of sediment), calculated from the Shields critical boundary stress Θ_c (Shields, 1936).

ρ is the water density estimated as 1023.6881 kg/m^3 (1.0239808 g/cm^3), at 3.5% (35 ppt) salinity and 24°C (ITTC, 2011).

$$\theta_c = \frac{\tau_0}{(\rho - \rho_w)gD}$$

Θ_c is obtained using the Shields diagram from the calculated boundary Reynolds number (Shields, 1936).

$$R_e = \frac{D}{v}\sqrt{(0.1gD(\frac{\rho}{\rho_w} - 1))}$$

R_e is the boundary Reynolds number. v is the kinematic viscosity. g is gravitational acceleration. ρ is the sediment density. ρ_w is the water density (Shields, 1936). For R_e > ~30 (which holds for initiation of sediment motion at Site 3), laboratory studies indicate $\Theta_c \approx 0.04$ (Garcia, 2008), which is the value that is applied here.

The above calculation has been done for D_{50} and D_{84}, which are defined as the size of particle for which 50% and 84% respectively of the sample is finer, by weight.

2.2 ADCP Data

2.2.1 Collection and Processing Methods

NOAA, through the Tampa Bay Physical Oceanographic Real-Time System (PORTS), has maintained a bottom-mounted vertical Acoustic Doppler Current Profiler (ADCP) deployed in the shipping channel under the Skyway Bridge. Within the 2000–2017 17-year study period, the ADCP had 9 deployments with varying positions and deployment time periods available from C-MIST. The ADCP is a Teledyne RDI Workhorse that operates at 1200 kHz (Dusek et al., 2017) and has a resolution of 0.1 cm/s sampled at a six minute interval (NOAA, 2013). The ADCP collects velocity data throughout the water column, divided into 11 1-m depth bins, where bin 1 (at a tidally averaged depth of 12.9 m for recent ADCP deployments) is deepest and bin 11 is shallowest (Dusek et al., 2017). The ADCP during one deployment additionally collected pressure data at a resolution of 0.1 m at a sample interval of 6 minutes. The pressure data are used herein for water level analyses.

2.2.2 Velocity Analysis Methods

Using MatLab, these data were converted from degrees north to referencing the axial (62 degrees) and co-axial (152 degrees) direction of the shipping channel under the Skyway Bridge with positive velocities indicating flood tide and negative velocities indicating ebb tide (Figures 6 and 7).

After historical data from 2000–2015 were processed, bin 5 was chosen to represent the mean flow velocity for comparison to the calculated fluid velocity to initiate sediment transport. ADCP data collected after 2015 were only processed using bin 5. The water depth at Site 3 is approximately 14.5 m, and bin 5 is centered at 8.9 m depth, so bin 5 is approximately 5.6 m above the bed.

2.2.3 Water Level Analysis Methods

Tidal data from Station 8726384 at Port Manatee were investigated for suitability or tidal correction on bathymetric data in the study area. This tide gauge is the geographically closest tide gauge to the study area. Station 8726384 tide gauge has a resolution of 0.001 m at a sample interval of 6 minutes. The acoustic Doppler current profiler (ADCP) pressure sensor data have a resolution of 0.1 m at a sample interval of 6 minutes. Data from this tide gauge are advantageous as the tide gauge is calibrated to the datum for mean lower low water (MLLW); and when compared to the ADCP the tide gauge data are both higher resolution and more continuous than the recorded PORTS data (NOAA, 2013). To calculate the tidal lag and amplitude corrections needed to use the tide gauge data for tidal correction of multibeam bathymetry data, the tide gauge data were compared to the pressure sensor data on the ADCP located in the study site over the entire year of 2004.

2.3 Multibeam Echosounder Data

2.3.1 Collection and Processing Methods

This study utilizes two multibeam echosounder (MBES) systems, a high-resolution Kongsberg Simrad EM3000 and a high-resolution Reson Seabat 7215. Both have been used to collect bathymetric

and backscatter data in the ship channel beneath the Skyway Bridge. These data were collected episodically from 2001 to 2011 with the EM 3000 and from 2015 to 2017 with the Seabat 7125.

The EM 3000 is a 300-kHz multibeam swath sonar with 127 overlapping 1.5 ° × 1.5 ° beams, producing a 130 ° swath. The EM 3000 was pole-mounted on the port side of the R/V *Suncoaster* for these surveys. Navigation and motion compensation were collected with a TSS brand (now Applanix) POS MV 320-V2. The POS MV consists of an inertial motion unit (IMU) and a global positioning system (GPS) azimuth measurement system (GAMS) including two GPS receivers. A Sea Bird CTD was used for sound velocity profile (SVP) correction.

The Reson SeaBat 7125 is a dual-frequency multibeam swath sonar with 512 overlapping beams that can be operated at 400 or 200 kHz. For this study the SeaBat7125 was operated at 400 kHz with a 140° swath which provides an across-track receive beam width of 0.5° and an along-track transmit beam width of 1°. The SeaBat 7125 was pole-mounted on the port side of the R/V *Bellows* while collecting 6 out of 7 datasets used in this study. Navigation and motion compensation data were collected with the Applanix POS MV OceanMaster system with Fugro Marinestar, which utilizes dual frequencies and up to 4 satellite constellations, enabled (Fugro, 2016). The POS MV OceanMaster consists of hardware similar to the 320-V2, with improved computing capabilities, software, satellite constellation options, and post-processing compatibility. The POS MV OceanMaster with Marinestar enabled has a horizontal accuracy of 10 cm with 95% certainty and a vertical accuracy of 15 cm with 95% certainty (Applanix, 2017). The roll and pitch have a 0.01 deg accuracy. An AML Oceanographic Minos•X with an SV•Xchange sound velocity sensor was used for sound velocity profile correction. The maximum total propagated uncertainty (TPU) was 3.8 cm (Figure 8).

Multibeam bathymetric data were episodically collected in the shipping channel under the Skyway Bridge with the EM 3000 between 2000 and 2009, and with the SeaBat 7125 beginning in 2015. Both of these systems are capable of exceeding IHO order 1A standards for bathymetric surveys. The bathymetry data were post processed according to IHO standards (IHO, 2008) using Caris HIPS and SIPS 10.2. The data have been tide-corrected to mean lower low water (MLLW) from the NOAA tide gauge

8726384 located at Port Manatee (27° 38.3'N, 82° 33.8'W). The bathymetric data herein meets or exceeds IHO order 1A standards. Bathymetry data collected with the EM 3000 were processed to a 2 m x 2 m swath angle grid. Bathymetry data collected with the Seabat 7125 were processed to a 0.5 m x 0.5 m CUBE and swath angle grid, the swath angle grids were used here in for analyses.

Backscatter mosaics were created for the September 2004 (300 kHz) and September 2015 (400 kHz) MBES surveys using the Caris SIPS Time-Series algorithm. A beam pattern was created for each survey using the Caris SIPS Create Beam Pattern tool, which utilizes the entire survey to extract a beam pattern. The mosaic was corrected for temperature, salinity, and beam pattern. Angular dependence was amended using the Caris SIPS AVG correction with a sliding window of 200 pings, and a swath-angle bathymetry surface was used to calculate incidence angle corrections. The mosaics for the 2004 and 2015 surveys were created on a 1.0 m and 0.01 m grid, respectively.

2.3.2 Bathymetry and Backscatter Analysis Methods

Backscatter Analysis

Backscatter mosaics were imported to ArcGIS for comparison to each other and to sediment sample locations and analyses (Figures 9 and 10). Trends and patterns in the backscatter mosaics were visually analyzed and compared. These mosaics cannot be compared quantitatively because as neither MBES system have calibrated backscatter, nor were they collected at the same frequency (Lurton et al., 2015).

Bathymetry Analysis

Volume changes within Area 1 (yellow box in Figure 3), including surveys from 2000 to 2017 from both MBES systems and located north of the center of the ship channel beneath the Skyway Bridge, were calculated using the Surface Difference tool in Fledermaus. The Surface Difference tool calculates volumes between two gridded bathymetry surfaces by summing the volumes of each individual cell and

calculating the difference. For the purposes of this study, average depth change over the entire area of Area 1, around the center of the ship channel beneath the Skyway Bridge, was calculated and graphed over time, using the September 2015 gridded bathymetry surface as zero for comparison (Figure 11). The same volume change analysis was conducted for Area 2 using the seven 400 kHz surveys collected in that area from 2015 to 2017, shown as an orange line in Figure 11. The volume difference between surveys were calculated (Table 1)**.** Discrepancies were noted between Areas 1 and 2 in May 2016, while other surveys during the 2015–2017 time period follow a similar trend in Areas 1 and 2. Large changes in volume in 2003 and 2004 were also observed. Due to these large changes, further bathymetric analysis was not completed in Area 1.

Bathymetry grids in Area 2 were further analyzed using tools from the Spatial Analyst Toolbox in ArcGIS Desktop 10.5. Surface change analyses were completed between each consecutive 400 kHz bathymetry survey between 2015 and 2017 using the Minus tool from the Spatial Analyst Math toolset, and a new difference raster was created for each (Figure 12). For each difference raster, mean, minimum, maximum, and standard deviation were calculated. Using each pixel within each difference raster, percent coverage of positive and negative change were calculated (Table 2). Slope was calculated as the derivative of each gridded bathymetry surface with a Z factor of 1 (meaning horizontal units to vertical units is 1:1), using the Slope tool from the Surface Toolset within the ArcGIS Spatial Analyst toolbox. A slope raster was also created for each survey using the Slope tool (Figure 13). Curvature, calculated as the second derivative of bathymetry, was calculated using the Curvature tool from the Surface toolset within the ArcGIS Spatial Analyst toolbox, with curvature rasters also created for map-view visualization (Figure 14). Profile curvature was calculated as the second derivative of bathymetry perpendicular to bathymetry contours, or curvature along-slope. Planform curvature was also calculated, as the second derivative of bathymetry parallel to contours, or curvature across-slope. Profile curvature and planform curvature were calculated and rasters were created using the same Curvature tool in the Spatial Analyst Surface toolset (Figure 15). Slope, curvature, profile curvature, and planform curvature were also derived from bathymetry of the 300 kHz MBES survey completed in 2004, which also covers Area 2 (Figure 16).

Statistics including minimum, maximum, mean values, and standard deviation were calculated within the layer properties in ArcGIS for each depth, slope, curvature, profile curvature, and planform curvature raster from the 400 kHz MBES surveys within Area 2 (Table 3). The same statistics were calculated for the rasters derived from the 2004 300 kHz MBES survey, to be compared with the combined statistics of the 400 kHz surveys (Table 4).

Continuous wave crests within Area 2 were manually traced within ArcGIS using 0.1 m contours as a guide (Figure 17). Wave crests from surveys in 2016 were of consistent enough shape for possible tracking over time (Figure 18). Distance between consecutive wave crests from surveys in 2016 were measured along the axial center line of the ship channel using the Measure tool in ArcGIS and mean calculated with positive values representing average crest movement into the bay and negative values representing crest movement out of the bay (Table 5).

The axial center of the ship channel and Area 2, a 75 m long line, was selected for wave-form analyses of the sand wave bedforms, as the wave crests were most consistent near the center of the channel. Depths along this line were extracted from the 7 bathymetry surveys conducted post 2014 and the October 2004 surveys using the Caris HIPS and SIPS profile tool. The bathymetric profiles were detrended and a fast Fourier transform was performed. The fast Fourier transform resulted in a spectra graph and periodogram for each profile (Figures 19 and 20). The average wave height, mean peak, and mean trough were calculated from each profile (Figure 21).

3. RESULTS

3.1 Sediment Samples

3.1.1 Sediment Analysis Results

Calcium carbonate content ranges from 25% to 87% (Figure 4, Table 6). The calcium carbonate content is greatest at Sample Site 3 at 87.6%; the sample taken from the center of the channel, and smallest at Sample Site 2 at 25.9%. Carbonate content at Sample Site 1 was 38.1% and carbonate content at Sample Site 4 was 68.1%. Results of the grain size analyses are shown in Figure 5 and Table 6. Mean grain size ranges from 0.01 φ (0.99 mm, coarse sand) at Sample Site 3 to 1.55 φ (0.34 mm, medium sand) at Sample Site 1 (Figure 5, Table 6). The smallest grain size, clay, ranged from 0.00% at Sample Sites 2 and 3 to 0.04% at Sample Site 1. The largest grain size, very fine gravel, ranged from 34.4% at Sample Site 3 to 11.2% at Sample Site 1. Grain size proportions are also shown in Figure 4, and distributions are shown in Figure 5. The D_{50} and D_{84} grainsize percentiles, at Sample Site 3, are 0 φ or 1.0 mm, and -1.5 φ or 2.8 mm, respectively.

3.1.2 Critical Shear Stress Analysis Results

The mean current velocity, U, required to initiate transport is calculated for the D_{50} grain size, in this case 0 φ or 1.0 mm, and for the D_{84} grain size percentile, in this case -1.5 φ or 2.8 mm. With a sand grain density of 2700 kg/m^3 and Θ_c = 0.04, the shear velocity to initiate transport for D_{50} and D_{84} are μ_* = 0.026 m/s and μ_* = 0.043 m/s, respectively. It then follows from applying the law of the wall equation at y = 5.6 m that for D_{50}, the critical velocity is U = 0.70 m/s, while for D_{84}, U = 1.05 m/s.

3.2 ADCP Data

3.2.1 ADCP Velocity Analysis Results

Velocities in the ship channel beneath the Skyway Bridge are greatest during spring tides (Figure 7). The dominant velocity direction is channel-axial, and the ebb tide reaches faster velocities than the flood tide. The calculated D_{84} critical velocity of 105 cm/s (indicated by a red line in Figure 7) is occasionally reached during spring ebb tides. However, the calculated D_{50} critical velocity of 70 cm/s (indicated by a green line in Figure 7) is reached by many peak flood and peak ebb currents during typical conditions or stronger (Figure 7). This suggests that the sand has been sorted by the dominant velocities such that bedload transport regularly occurs.

3.2.2 Water Level Analysis Results

Over the year analyzed, no significant time difference between high tides and low tides were found between the PORTS ADCP sensor and the Port Manatee tide gauge. Typical results of the analysis are shown in Figure 22. The difference between peak amplitude is attributed to the higher resolution of the tide gauge data. As a result of these analyses, the Port Manatee tide gauge MLLW data were used for multibeam bathymetry tidal correction, without requiring a phase lag or amplitude scalar.

3.3 Multibeam Echosounder Data

3.3.1 Backscatter Analysis Results

Backscatter mosaics from both 2015 and 2004 (Figures 9 and 10) show slightly higher backscatter values on the sand waves at the center of the channel, with the highest backscatter beneath the Skyway Bridge, and slightly lower backscatter to either side of the channel center. Both mosaics show more homogenous backscatter intensities southwest of the Skyway Bridge relative to that beneath the bridge and to the northeast, on the Tampa Bay side. Linear features parallel to the channel beneath the

bridge are present in both the 2004 and 2015 backscatter mosaics. Both mosaics also exhibit a splotchy pattern of backscatter on the south side of the channel, northeast of the bridge. As no distinct zonation of backscatter is apparent, it is difficult to draw conclusions from the backscatter alone.

3.3.2 Bathymetric Analysis Results

Average Depth Analysis

Average depth in Area 1 between 2000 and 2017 ranged from -0.42 m to 2.8 m relative to the September 2015 survey, which was set to be zero (Table 1, Figure 11). Change between average depths in Area 1 between 2000 and 2017 averaged 0.034 m, ranging from -1.9 m to 2.1 m. Average depth in Area 1 between 2000 and 2009 (300 kHz datasets) ranged from -0.42 m to 2.8 m, with a standard deviation of 0.79 m. Average depth of Area 1 between 2015 and 2017 (400 kHz datasets) ranged from -0.31 m to 0.26 m, with a standard deviation of 0.19 m. Change between average depths in Area 1 between 2000 and 2009 averaged 0.073 m, ranging from -1.9 m to 2.1 m, with a range of 4 m and a standard deviation of 0.91. Change between average depths in Area 1 between 2015 and 2017 averaged -0.037 m, ranging from -0.52 m to 0.23 m, with a range of 0.75 m and a standard deviation of 0.29 m.

Average depth in Area 2 between 2015 and 2017 (400 kHz datasets) ranged from -0.36 m to 0.6 m relative to the September 2015 survey. Change in average depth in Area 2 between 2015 and 2017 ranged from -0.98 m to 0.64 m, averaging 0.049 m with a standard deviation of 0.61 m.

Surface Change Analysis

The average of the average difference surfaces in Area 2 is 0.35 m with a maximum of 0.69 m and a minimum of 0.14 m (Table 2). The average minimum surface difference is -1.03 m with a minimum of -0.42 m and a maximum of -1.23 m. The average maximum surface difference is 1.09 m with a maximum of 2.1 m and a minimum of 0.67 m. The average standard deviation of the difference surfaces is 0.35 m with a maximum of 0.69 m and a minimum of 0.14 m. Percent of positive pixels averaged 0.48

with a minimum of 5.23 percent and a maximum of 80.25 percent. Percent of negative pixels averaged 0.51 with a minimum of 19.74 percent and a maximum of 94.76 percent.

Positive and negative change between surveys follow sand wave trends (Figure 12). With the exception of change before and after the May 11, 2016 survey, more positive and more negative change alternate in the axial direction. Between the November 20, 2016 and May 11, 2016 surveys, change is very positive to the southeast, and negative to the northwest. Between the May 11, 2016 and June 27, 2016 surveys, change is very negative to the southeast and positive to the northwest.

Slope Analysis

The average of the average slope of all surveys within Area 2 is 10.3 degrees with an average minimum of 9.30 degrees and an average maximum of 11.1 degrees (Tables 3 and 4). The slope surfaces have an average standard deviation of 5.31 degrees with a minimum standard deviation of 4.96 degrees and a maximum of 5.64 degrees. The Kongsberg October 23, 2014 survey's slope spatial analysis has a minimum of 0.18 degrees, a maximum of 21.3 degrees, a mean of 7.41 degrees, a standard deviation of 3.90 degrees (Table 4), and a similar character to the 2015-2017 surveys' slope spatial analysis (Figures 13 and 16b).

Curvature Analysis

The average of the average curvature of all surveys within Area 2 is 0.00 cm with an average minimum of -458 cm and an average maximum of 432 cm (Tables 3 and 4). The mean standard deviation of the curvature surfaces is 53.8 cm. The minimum curvature is -1560 cm occurring in November 20, 2015 survey. The minimum curvature standard deviation is 492 cm. The maximum curvature is 945 cm also occurring in the November 20, 2015 survey. The maximum curvature standard deviation is 234.47 cm. The Kongsberg October 23, 2014 survey's curvature spatial analysis has a minimum of -215 cm, a maximum of 228 cm, a mean of 0 cm, a standard deviation of 45.6 cm (Table 4), and is spatially of similar character to the 2015-2017 surveys' curvature spatial analysis (Figures 14 and 16c).

Profile and Planform Curvature Analysis

The average of the average profile curvature of all surveys within Area 2 is 0.37 cm with an average minimum of -240 cm and an average maximum of 255 cm (Tables 3 and 4). The mean standard deviation of the profile curvature surfaces is 34.9 cm. The minimum profile curvature is -627 cm occurring in the November 20, 2015 survey. The minimum profile curvature standard deviation is 174 cm. The maximum profile curvature is 782 cm also occurring in the November 20, 2015 survey. The maximum profile curvature standard deviation is 232 cm.

The average of the average planform curvature of all Area 2 surveys is 0.370 cm with an average minimum of -230 cm and an average maximum of 269 cm. The mean standard deviation of the planform curvature surfaces is 26.0 cm. The minimum planform curvature is -781 cm occurring in the November 20, 2015 survey. The minimum planform curvature standard deviation is 246 cm. The maximum planform curvature is 767 cm occurring in the November 20, 2015 survey. The maximum planform curvature standard deviation is 221 cm. The October 23, 2004 survey's profile curvature has a minimum of -114 cm, a maximum of 124 cm, a mean of 1.75 cm, a standard deviation of 26.1 cm (Table 4), and has similar character to the 2015-2017 surveys' profile curvature spatial analysis (Figures 15 and 16d-e). The October 23, 2004 survey's planform curvature spatial analysis has a minimum of -121 cm, a maximum of 138 cm, a mean of 1.75 cm, a standard deviation of 23.9 cm (Table 4), and a similar character to the 2015-2017 surveys' curvature spatial analysis (Figures 15 and 16d-e).

Wave Crest Analysis

When measured along the cross-section profile line, wave crests observed within the May 11, 2016 and June 27, 2016 surveys moved an average of 0.84 m, with a standard deviation of 0.36. Flood direction, towards the northeast and into the bay, is positive as in the ADCP analysis (Table 5). Wave crests between the June 27, 2016 and July 17, 2016 surveys moved an average of 0.49 m with a standard deviation of 0.35. Between the July 17, 2016 and September 14, 2016 surveys, wave crest moved an average of -0.55 m with a standard deviation of 0.50. During each time period, most wave crests moved in

the same direction as each other, though one wave crest between June 27, 2016 and July 17, 2016 and two wave crests between July 17, 2016 and September 14, 2016 moved in the opposite direction of the other sand waves during their respective time periods (highlighted in Table 5).

In map view, wave crests within Area 2 shift from trending north-south in September 2015 to trending north-northwest to south-southeast in April 2017 (Figure 17). It is not always conclusive to identify individual wave crests between surveys with longer time intervals, but the surveys conducted in 2016 were temporally close, such that wave crests were easily identifiable between surveys (Figure 18). During the 2016 surveys, most of the wave crests retained their shape. Wave crests bifurcate, detach, and reattach to a different wave crest, apparent in wave packets 4a-4b in Figure 18. These types of changes are too great between other surveys to trace wave crests.

Wave Form Analysis

The primary spatial wave frequency for all surveys ranged between 0.13 m^{-1} and 0.22 m^{-1} (Figure 19). The primary wave period for all surveys ranged between 4.5 m and 6.0 m (Figure 20). The surveys between 2015 and 2017 showed an average wave height of 0.45 m, an average peak of 0.26 m with a standard deviation of 0.09 m, and an average trough of -0.18 m with a standard deviation of 0.06 m. The October 2004 surveys showed an average wave height of 0.51 m, an average peak of 0.31 m with a standard deviation of 0.11 m, and an average trough of -0.20 m with a standard deviation of 0.06 m (Table 6 and Figure 21). The maximum bedform wave height along the axial cross-section analyzed is 0.8 m, observed in the April 21, 2017 survey. However, sandwaves with wave heights of about 1 m are observed outside of the Area 2 and off the axial center.

4. DISCUSSION

4.1 Character of the Sandwaves

Grain size and carbonate fraction vary amongst the four sample sites. Sample Site 1 is located within the shipping channel southwest of the Skyway Bridge (on the Gulf of Mexico side) and south of the channel thalweg. Backscatter in this location is homogenous and of medium intensity in both 2015 and 2004, and the bathymetry is smooth. Sediment samples from Site 1 consist of mostly medium and fine sand, and have the second-lowest carbonate content of the four samples.

Sample site 4 is located northeast of the bridge (on the Tampa Bay side), and north of the channel thalweg. This sample is located in a lower-intensity area of backscatter than the other three sample sites, in both 2015 and 2004. Sediment from Sample Site 4 consists of a well-mixed variety of coarser grain sizes, including fine sand, medium sand, coarse sand, very coarse sand, and fine gravel. This sediment also has the second-largest carbonate content of the four samples.

Sample Site 2 is located beneath the Skyway Bridge, south of the channel thalweg, within what is likely to be a scoured hole, visible in the bathymetry. Sediment from Sample Site 2 is bimodal in size distribution, consisting of mostly fine siliciclastic sand, and very fine carbonate gravel, with the lowest carbonate content of the four samples at 25.95%. A low volume of sediment was recovered from this site, indicating that there is likely exposed hard bottom at this location. Currents directly beneath the Skyway Bridge are likely higher than to either side of the bridge as the channel is constricted by the bridge structure. Ledges on the southern edge of this hole indicate erosion, and are the only part of the hole apparent in backscatter, likely due to a shadow effect. Linear features in the backscatter, parallel to the channel beneath the bridge correspond to ledges in the bathymetry, possibly eroded due to the higher velocity currents in the restricted part of the channel.

Sample Site 3 is located in the center of the channel, northeast of the Skyway Bridge within the sandwave field that dominates the center of the shipping channel near the bridge. In this location, backscatter intensity in both the 2015 and 2004 surveys is higher than the surrounding channel, but not as high as the channel center directly beneath the bridge. Of the four sites sampled, Sample Site 3 is the most representative of the sandwaves beneath the Skyway Bridge. Of the four sample sites, sediment from Sample Site 3 is the coarsest by volume, dominated by coarse sand and very fine gravel, and has the highest carbonate content (87.6%). Sediment size from this sample site are bimodal distributed. Brooks and Doyle (1998) found the mean grain size of the surface sediments adjacent to the study area were between 2 φ and 1.5 φ and carbonate content between 60% and 65%. This is consistent with the mean grain size and carbonate content found on the edges of the shipping channel, Sample Sites 1 and 4. However the sediments grain size comprising the sandwave bedforms, Sample Site 3, has a mean grain size of 0.01 φ and a carbonate content of 87%, larger than the surrounding bay. The larger grain size of the bedforms indicates that the sediments have been winnowed by higher velocity currents. The winnowed sediments likely account for the higher backscatter intensity in the sandwaves beneath the bridge, present in both the 2015 and 2004 backscatter intensity mosaics. As relative backscatter intensity in these four locations is similar in both the 2015 and 2004 surveys, despite differing systems and frequencies, the sediment distribution pattern within this shipping channel likely did not change significantly in the 11 years between 2004 and 2015.

This study shows that sandwave bedforms under the Skyway Bridge are in a state of equilibrium over the 13-years observed in this study. Motion of the bedforms does occur; this motion is complex and deserves further investigation at a higher temporal resolution. However, the bedforms between October 2004 and April 2017 are consistent in wavelength and wave height over a 13-year time period. Despite significant outliers in both the 2000–2009 data and the 2015–2017 data, the average depth of the bedforms changes little. Comparing the slope, curvature, planform curvature, and profile curvature histograms from both the 2004 survey and the post-2014 surveys; the histograms are of similar shape and character (Table 4). The spectragram shows that the waveforms in both surveys in 2004 have primary

frequencies within the maximum and minimum primary frequencies of the waveforms in the post-2014 surveys (Figure 19).

Motion of the wave crests is observed between all surveys (Figures 17 and 18). The amount of motion is unsurprisingly correlated with the amount of time between surveys. Due to the coarse grain size of the sediment comprising the waveforms, the waveforms while in motion only move on average under 1 m per month. This motion is not always in a singular direction. Had only two surveys in this study been conducted, as in Ernstsen et al. (2005), bed load transport in either direction could have been supported, depending on the timing of the two surveys. Individual wave crest motion is observed in adjacent surveys both in the flood direction and ebb directions. While it was expected that the primary bedform motion would be in the ebb direction caused by the relatively faster spring ebb current velocities, this pattern is not always observed. Unfortunately due to a large gap in the ADCP data during the summer of 2016 (Figure 7), insight into the motion of these bed forms during that time is unavailable. More frequent surveys with concurrent and continuous ADCP data would provide higher temporal resolution and greater insight into the evolution of these bedform morphologies.

The May 11, 2016 survey is an anomalous result. The average depth within Area 2 is not in agreement with the average depth within Area 1 with a 0.93 m difference. The average depth of Area 2 from the May 11, 2016 survey is an outlier when compared to Area 2 from other 2015–2017 surveys. Compared to the surveys before and after, the surface of the May 11, 2016 survey seems to be tilted along an axial axis, as evidenced by the positive surface change to the southeast and negative surface change to the northwest between November 20, 2015 and May 11, 2016 and vice versa between May 11, 2016 and June 27, 2016 (Figure 12). It was later discovered that the sonar head moved during the transit, which likely accounts for this discrepancy. The bathymetry derivative surfaces from both 2015 surveys have larger extreme values when compared to the 2016 surveys. This is an artifact in the data caused by the combination of adjacent survey lines, whereas all surveys conducted during 2016-2017 were single track lines.

4.2 Comparison to Tidally-influenced Sandwave Bedforms around the World

Like the channel beneath the Skyway Bridge, the Adolphus Channel in Australia is a tidally-influenced shipping channel, with similar depths; the Adolphus Channel is mostly less than 20 m deep (Harris, 1988). The bed of the Adolphus Channel also consists of sandwaves and scoured rock, though the carbonate content of the sediment is higher at 94-96%, while the sediment in the shipping channel beneath the Skyway Bridge has a maximum carbonate content of 87.65%. The average grain size in the Adolphus Channel is 0.32 ϕ (0.80 mm) while the average grain size of the sediment comprising the sandwaves beneath the Skyway Bridge is larger at 0.01 ϕ (0.99 mm). Sandwaves in the Adolphus Channel, Australia, average 0.75 m of bedform movement per day, between two surveys one month apart (Harris, 1988). Average wavelength in the Adolphus Channel during the two surveys was 101 m (Harris, 1988), much longer than the average wavelength of 5.2 m in this study area. This yields a 0.74% bedform movement per day as a percentage of the wavelength for scaled comparison to this study.

A large sandwave field outside the mouth of San Francisco Bay covers an area of 4 km^2 that has wavelengths up to 220 m and wave heights up to 10 m (Barnard et al., 2006). Not only are the tidally-influenced sandwaves placed differently in the bay setting, they are over an order of magnitude larger than the sandwaves present in the shipping channel at the entrance to Tampa Bay. The San Francisco Bay sandwaves average 1.7 m of movement per day, over five surveys in a one-month study period. (Wayman, 2005). Average wavelength in a small repeat study area is about 80 m, with an average amplitude of about 6 m (Wayman, 2005). This yields a 2.1% bedform movement per day as a percentage of the wavelength.

The entrance to Gironde estuary in France is also tidally-influenced with axial velocities, also measured via ADCP, up to 1.30 m/s measured 1 m above the bed (Berné et al., 1993) whereas the maximum axial current velocity of most tidal cycles during spring tide measured by the Tampa Bay PORTS ADCP in the study area are about 1 m/s; 23% less. Both have limited wave action but the estuary has more river discharge influence on flow and sediment supply. The sediment at the Gironde estuary was not analyzed for grain size or carbonate content in Berné et al. (1993). Between two surveys June 1, 1987

and October 14, 1989 (866 days) crests of dunes moved downstream 20 m (eastern) to 40 m (western part), mean wave height 4.2 m, mean trough to trough spacing 84.0 m, (Berné et al., 1993). Per day the bedforms are moving 0.055% of the wavelength.

The Skyway sandwaves have wavelengths an order of magnitude smaller than sandwaves found in the Adolphus Channel, the mouth of San Francisco Bay, and the Gironde estuary. However, by comparing the scaled motion of each of these studies as a calculated percent of wavelength per day to this study's calculated range of 0.4% between the June 27, 2016 and July 17, 2016 surveys, and -0.17% between the July 17, 2016 and September 14, 2016 surveys, we find that they are comparable. The sandwaves of San Francisco Bay and the Gironde estuary have percent motion one order of magnitude larger and smaller, respectively, than this study area in Tampa Bay. Scaled motion of sandwaves in the Adolphus Channel is of the same order of magnitude as sandwaves in this study. Due to the large number of surveys over time, it is also apparent in this study, however, that the sandwaves are moving in both flood and ebb directions, rather than in the same net direction over time. It is therefore difficult to compare the rate of movement to other studies which assume movement in one net direction over time between two surveys (Harris, 1988; Berné et al., 1993). This study has also shown that sediment transport, related to current velocity varies on several time scales with tidal cycles and moon phases (Figure 7). Thus, simply calculating a daily movement rate of sandwaves between surveys as in Wayman (2005) and Harris (1988) is not necessarily representative of daily sandwave migration or bedload transport.

4.3 Future Work

To better understand the bedform dynamics of the shipping channel near the Skyway Bridge, frequent surveys are needed before and after spring flood and ebb tides with concurrent ADCP data. With this information we will be able to discern how much these bedforms are moving on a daily and monthly basis and have a better estimate of what flow velocities are needed for these bedforms to migrate. Additionally, improved estimates for y_0 (height above the bed where mean flow is zero) would improve

the critical shear stress calculations. A study of the Skyway sediment particle dynamics and interactions would provide any additional future work in this area with important parameters that would describe sediment transport, such as saltation and armoring effects. With the appropriate parameters and boundary conditions along with the observations herein, a 3D model could be created and tested to model bedform migration. These data herein could be used to both force and test the model. This model would be a useful tool for dredging operations and channel maintenance, as well as aid channel navigation, and hurricane impact assessments and recovery. A post-Hurricane Irma survey was conducted on October 17, 2017. Comparing and analyzing this survey with the analysis done here in may increase understanding of how hurricane Irma affected Tampa Bay. A survey and analysis of the bedforms after channel-widening is completed would be beneficial to assess how the change in channel width affects current velocities, bedform morphologies, and sediment transport in the Skyway Bridge setting.

5. CONCLUSIONS

The shipping channel beneath the Skyway Bridge contains sandwave bedforms along the center of the channel that consist of coarser grain sizes (0.01 φ) and higher carbonate content (87.6%) than the surrounding channel and natural bay. Relative backscatter intensity distribution indicates that the sediment distribution pattern within the shipping channel has not significantly changed between 2004 and 2015. Higher backscatter intensity and grain size from sandwaves beneath the Skyway Bridge suggests that higher-velocity currents in the restricted channel beneath the bridge result in winnowed sediments. Currents reach the calculated D_{50} critical shear stress velocity of 70 cm/s to initiate transport of this sediment frequently during both peak flood and ebb currents, except during neap tides. The D_{84} critical shear stress is reached intermittently, mostly during spring tides. The predominant wavelength of sandwaves within the study area is about 5 m, with an average wave height of 0.47 m. Derivatives of bathymetry including slope, curvature, and profile and planform curvature, are consistent in range, value, and spatial distribution through time despite uncertainty in absolute depth.

The bedforms in the shipping channel under the Skyway Bridge are consistent in size and shape over a span of 13 years. The sandwaves are dynamic, migrating episodically with spring tidal currents, but tend to maintain a characteristic size, wave height, and wavelength. Higher temporal resolution over two years shows that these sandwaves move in both the ebb and flood directions. This indicates that only two surveys is not enough to determine sediment transport over time in a tidally-influenced environment. More consistent and temporally smaller multibeam echosounder survey intervals and more continuous ADCP data availability would allow for better understanding of sediment transport via bedform migration in tidally-influenced environments.

REFERENCES

Afzalimehr, H., & Rennie, C. D. (2009). Determination of bed shear stress in gravel-bed rivers using boundary-layer parameters. *Hydrological Sciences Journal*, *54*(1), 147-159.

AAPA. (2016). U.S Port Rankings by Cargo Tonnage 2016. American Association of Port Authorities. Alexandra, Virginia. Accessed January 28, 2018. http://www.aapa-ports.org/unifying/content.aspx?ItemNumber=21048#Statistics

Applanix, A Trimble Company. (2017). POS MV Oceanmaster Specifications. Ontario, Canada. https://www.applanix.com/downloads/products/specs/posmv/POSMV_OCEANMASTER.pdf

Barnard, P. L., Hanes, D. M., Rubin, D. M., & Kvitek, R. G. (2006). Giant sand waves at the mouth of San Francisco Bay. *Eos, Transactions American Geophysical Union*, 87(29), 285-289.

Bates, R. L., & Jackson, J. A. (Eds.). (1984). *Dictionary of geological terms* (Vol. 584). Anchor Books.

Berné, S., Castaing, P., Le Drezen, E., & Lericolais, G. (1993). Morphology, internal structure, and reversal of asymmetry of large subtidal dunes in the entrance to Gironde Estuary (France). *Journal of Sedimentary Research*, *63*(5).

Biron, P. M., Lane, S. N., Roy, A. G., Bradbrook, K. F., & Richards, K. S. (1998). Sensitivity of bed shear stress estimated from vertical velocity profiles: The problem of sampling resolution. *Earth Surface Processes and Landforms*, *23*(2), 133-139.

Brooks, G. R., & Doyle, L. J. (1998). Recent sedimentary development of Tampa Bay, Florida: A microtidal estuary incised into tertiary platform carbonates. *Estuaries*, *21*(3), 391-406.

Dalrymple, R. W. (1984). Morphology and internal structure of sandwaves in the Bay of Fundy. *Sedimentology*, *31*(3), 365-382.

De Visser, A. (1997). *Sand Wave Study* (No. NFESC-TM-2261-OCN). Naval Facilities Engineering Service Center for Port Hueneme, California.

Doyle, L J., Brooks, G. R., Fanning, K. A., Van Vleet, E. S., Byrne, R. H., and Blake, N. J. (1989). A characterization of Tampa Bay sediments. *Reports*. Paper 108. http://scholarcommons.usf.edu/basgp_report/108

Dusek, G., Park, J., and Paternostro, C. (2017). Seasonal variability of tidal currents in Tampa Bay, Florida. *Journal of Waterway, Port, Coastal, and Ocean Engineering*, *143*(3).

Einstein, H. A., & El-Samni, E. S. A. (1949). Hydrodynamic forces on a rough wall. *Reviews of modern physics*, *21*(3), 520.

Elias, E. P., & Hansen, J. E. (2013). Understanding processes controlling sediment transports at the mouth of a highly energetic inlet system (San Francisco Bay, CA). *Marine Geology, 345*, 207-220.

Ernstsen, V. B., Noormets, R., Winter, C., Hebbeln, D., Bartholomä, A., Flemming, B. W., & Bartholdy, J. (2005). Development of subaqueous barchanoid-shaped dunes due to lateral grain size variability in a tidal inlet channel of the Danish Wadden Sea. *Journal of Geophysical Research: Earth Surface, 110*(F4).

Folk, R. L. (1968). *Petrology of sedimentary rocks*. Hemphill Publishing Company. Austin, Texas.

Folks, J. L., & Antle, C. E. (1965). Optimum allocation of sampling units to strata when there are R responses of interest. *Journal of the American Statistical Association, 60*(309), 225-233.

Fugro. (2016). MarineStar Positioning Services. Leidschendam, Netherlands. https://www.fugro.com/docs/default-source/Our-Services/asset-integrity/marinestar-positioning-flyer.pdf

Garcia, M. H. (2008). Sediment transport and morphodynamics. In: M. H. García (Ed.), *Sedimentation Engineering: Processes, Measurements, Modeling and Practice*. American Society of Civil Engineers, Reston, Virginia (pp. 21-163).

Gibbs, R. J. (1974). A settling tube system for sand-size analysis. *Journal of Sedimentary Petrology, 44*(2).

Goodell, H. G., & Gorsline, D. S. (1961). A sedimentologic study of Tampa Bay, Florida. Report of the International Geological Congress, XXI, part XXIII. 75-88.

Goodwin, C. R. (1987). *Tidal-flow, circulation, and flushing changes caused by dredge and fill in Tampa Bay, Florida*. U.S. Geological Survey water-supply paper 2282. US Government Printing Office.

Harris, P. T. (1988). Large-scale bedforms as indicators of mutually evasive sand transport and the sequential infilling of wide-mouthed estuaries. *Sedimentary Geology, 57*(3-4), 273-298.

IHO (2008). *IHO Standards for Hydrographic Surveys*, 5th Edition. Special Publication No. 44, International Hydrographic Organization, Monaco.

ITTC (2011). *Fresh Water and Seawater Properties, Revision 02*. ITTC-Recommended Procedures and Guidelines Section 7.5-02-01-03, International Towing Tank Conference, Denmark.

Jackson, S., & Parker, A. (2017). Corps awards St. Pete / Tampa harbors maintenance dredging contract [U.S. Army Corps of Engineers News Release]. Published September 1. Retrieved from http://www.saj.usace.army.mil/Media/News-Releases/Article/1297519/corps-awards-st-pete-tampa-harbors-maintenance-dredging-contract/

Katoh, K., Kume, H., Kuroki, K., & Hasegawa, J. (1999). The development of sand waves and the maintenance of navigation channels in the Bisanseto Sea. In *Coastal Engineering 1998* (pp. 3490-3502).

Kironoto, B. A., & Graf, W. H. (1995). Turbulence characteristics in rough non-uniform open-channel flow. *Proceedings of the institution of civil engineers-water maritime and energy, 112*(4), 336-348.

Knaapen, M. A. F., & Hulscher, S. J. (2002). Regeneration of sand waves after dredging. *Coastal Engineering*, *46*(4), 277-289.

Krumbein, W. C., & Pettijohn, F. J. (1938). Manual of sedimentary petrography. Appleton-Century-Crofts, Inc., New York. 549 p.

Levin, D. R., Lillycrop, W. J., & Alexander, M. P. (1992). *Sand Waves. Report 1. Sand Wave Shoaling in Navigation Channels* (No. WES/TR/HL-90-17). Army Engineer Waterways Experiment Station, Vicksburg, MS Hydraulics Lab.

Lewis, D. W. & McConchie, D. (1994). Analytical sedimentology. New York, Chapman & Hall. 197p.

Lurton, X., Lamarche, G., Brown, C., Lucieer, V. L., Rice, G., Schimel, A., & Weber, T. (2015). Backscatter measurements by seafloor-mapping sonars: guidelines and recommendations. *A collective report by members of the GeoHab Backscatter Working Group*, (May), 1-200.

Milliman, J. D. (1974). *Marine Carbonates, Part I*. Heidelberg7 Springer-Verlag. Berlin, Heidelburg, New York. 378 p.

NOAA (2013). Sensor Specifications and Measurement Algorithms. NOAA's Ocean Service Center for Operational Oceanographic Products and Services (CO-OPS) Environmental Measurement Systems. Revised July 2013.

Redding, J. H. (2000). Experimental manipulation of sandwaves to reduce their navigation hazard potential, Jade shipping channel, N. Germany. In *Marine Sandwave Dynamics Workshop*. 23-24 March. Lille, France.

Rubin, D. M., & McCulloch, D. S. (1980). Single and superimposed bedforms: a synthesis of San Francisco Bay and flume observations. *Sedimentary Geology*, *26*(1-3), 207-231.

Shields, A. (1936). Application of Similarity Principles and Turbulence Research to Bed-Load Movement. California Institute of Technology, Pasadena (Translate from German).

Sterlini, F., Hulscher, S. J., & Hanes, D. M. (2009). Simulating and understanding sand wave variation: A case study of the Golden Gate sand waves. *Journal of Geophysical Research: Earth Surface*, *114*(F2).

Stolk, A. (2000). The role of sandwaves in the management of the Netherlands Continental Shelf. In *Marine Sandwave Dynamics Workshop* (pp. 199-200).

van Santen, R. B., De Swart, H. E., & van Dijk, T. A. G. P. (2011). Sensitivity of tidal sand wavelength to environmental parameters: A combined data analysis and modelling approach. *Continental Shelf Research*, *31*(9), 966-978.

van den Berg, J., Sterlini, F., Hulscher, S. J., & Van Damme, R. (2012). Non-linear process based modelling of offshore sand waves. *Continental Shelf Research*, *37*, 26-35.

Wayman, K. (2005). Bedform migration and sediment transport rates in the mouth of San Francisco Bay. *Unpublished MSc Thesis, California State University, Monterey Bay*.

Weisberg, R. H., & Zheng, L. Y. (2006). Circulation of Tampa Bay driven by buoyancy, tides, and winds, as simulated using a finite volume coastal ocean model. *Journal of Geophysical Research: Oceans*, *111*(C1), 899–913.

Yalin, M. S. (1964). Geometrical properties of sand wave. *Journal of the Hydraulics Division*, *90*(5), 105-119.

TABLES

Table 1. Average depth and average depth change for Analysis Areas 1 and 2 over time. Note varying date ranges and associated MBES systems. Note that maximum and minimum extremes (red), are entirely within the 300 KHz datasets, and the resulting high standard deviation of the 300 kHz and combined datasets compared to the 400 kHz datasets alone (bold).

	Analysis Area 1			Analysis Area 2
Date Range (MBES Frequency)	**2000-2017 (300 kHz and 400 kHz)**	**2000-2009 (300 kHz)**	**2015-2017 (400 kHz)**	**2015-2017 (400 kHz)**
Avaerage Depth (m)				
Mean	0.43	0.67	-0.05	0.05
Max	2.84	2.84	0.26	0.62
Min	-0.42	-0.42	-0.31	-0.36
Std. Dev.	**0.73**	**0.79**	**0.20**	**0.34**
Average Depth Change (m)				
Mean	0.03	0.07	-0.04	0.05
Max	2.08	2.08	0.23	0.64
Min	-1.86	-1.86	-0.52	-0.98
Std. Dev.	**0.74**	**0.91**	**0.28**	**0.61**

Table 2. Surface change analysis of bathymetry for 2015 to 2017 surveys in Analysis Area 2. Note large values surrounding the May 11, 2016 survey (red box). All dates are formatted month/day/year.

Reson Seabat 7125 (400 kHz) Analysis Area 2						
Date Range	**09/09/2015 to 11/20/2015**	**11/20/2015 to 05/11/2016**	**05/11/2016 to 06/27/2016**	**06/27/2016 to 0717/2016**	**07/17/2016 to 09/14/2016**	**09/14/2016 to 04/21/2017**
Surface Change (meters, positive up)						
Min	-0.62	-1.2	-2.8	-0.42	-0.41	-0.71
Max	0.85	2.1	1	0.84	0.67	1.1
Mean	-0.03	0.64	-0.97	0.22	0.13	0.23
Std. Deviation	0.17	0.66	0.69	0.14	0.15	0.29
Positive Change (# of pixels)	4790	9894	1027	645	9848	9696
Negative Change (# of pixels)	7544	2434	11253	11683	2549	2701
Total (# of pixels)	12334	12328	12280	12328	12397	12397
% Positive	38.836%	80.256%	8.363%	5.232%	79.439%	78.212%
% Negative	61.164%	19.744%	91.637%	94.768%	20.561%	21.788%

Table 3. Bathymetry analysis of Analysis Area 2 from 2015-2017 surveys including depth, slope, curvature, profile curvature, and planform curvature. All dates are formatted month/day/year.

Reson Seabat 7125 (400 kHz) Analysis Area 2							
Date	**9/9/2015**	**11/20/2015**	**5/11/2016**	**6/27/2016**	**7/17/2016**	**9/14/2016**	**4/21/2017**
Depth (m)							
Min	-16.0	-16.0	-16.5	-16.5	-16.1	-16.0	-16.0
Max	-13.8	-13.9	-13.0	-14.2	-14.0	-13.8	-13.5
Mean	-14.7	-14.8	-14.1	-15.1	-14.9	-14.7	-14.5
Std. Deviation	0.400	0.350	0.710	0.420	0.410	0.420	0.460
Slope (degrees)							
Min	0.120	0.030	0.110	0.090	0.110	0.150	0.080
Max	31.5	34.7	32.8	29.9	29.0	30.3	30.0
Mean	9.77	9.30	10.5	10.5	10.4	10.9	11.1
Std. Deviation	5.25	4.96	5.60	5.49	5.11	5.52	5.64
Curvature (cm)							
Min	-312	-1560	-379	-300	-188	-295	-170
Max	440	945	412	287	354	296	289
Mean	0.00	0.00	0.00	0.00	0.00	0.00	0.00
Std. Deviation	52.0	103	41.6	44.0	43.5	48.9	43.0
Profile Curvature (cm)							
Min	-234	-627	-206	-151	-154	-177	-134
Max	175	782	189	152	167	161	160
Mean	0.570	0.030	0.530	0.430	0.170	0.690	0.170
Std. Deviation	33.8	59.0	28.1	30.8	29.5	33.8	29.5
Planform Curvature (cm)							
Min	-167	-781	-190	-148	-104	-133	-85.3
Max	220	767	206	153	200	176	157
Mean	0.570	0.0300	0.530	0.430	0.170	0.690	0.170
Std. Deviation	25.5	51.0	20.6	20.9	20.9	22.6	20.4

Table 4. Combined bathymetry analysis of 2015 to 2017 surveys within Analysis Area 2 and bathymetry analysis of the 2004 survey collected with a different MBES system in the same area. Means of all 400 kHz surveys are in bold for comparison to the 300 kHz survey, also bold.

Reson SeaBat 7125 (400 kHz) Analysis Area 2 (all dates combined)					Kongsberg EM3000 (300 kHz) Analysis Area 2	
	Min	**Max**	**Mean**	**Std. Deviation**		**10/23/2004**
Depth (m)					**Depth (m)**	
Min	-16.5	-16.0	**-16.2**	0.228	**Min**	**-15.4**
Max	-14.2	-13.0	**-13.8**	0.384	**Max**	**-13.1**
Mean	-15.1	-14.1	**-14.7**	0.305	**Mean**	**-14.1**
Std. Deviation	0.350	0.710	**0.453**	0.118	**Std. Deviation**	**0.430**
Slope (degrees)					**Slope (degrees)**	
Min	0.0300	0.150	**0.0986**	0.0376	**Min**	**0.180**
Max	29.0	34.7	**31.2**	2.00	**Max**	**21.3**
Mean	9.30	11.1	**10.3**	0.611	**Mean**	**7.41**
Std. Deviation	4.96	5.64	**5.37**	0.262	**Std. Deviation**	**3.90**
Curvature (cm)					**Curvature (cm)**	
Min	-1560	-170	**-458**	492	**Min**	**-215**
Max	287	945	**432**	234	**Max**	**228**
Mean	0.00	0.00	**0.00**	0.00	**Mean**	**0.00**
Std. Deviation	41.6	103	**53.8**	22.2	**Std. Deviation**	**45.6**
Profile Curvature (cm)					**Profile Curvature (cm)**	
Min	-627	-134	**-240**	174	**Min**	**-114**
Max	152	782	**255**	232	**Max**	**124**
Mean	0.0300	0.690	**0.370**	0.247	**Mean**	**1.75**
Std. Deviation	28.06	58.98	**34.91**	10.84	**Std. Deviation**	**26.1**
Planform Curvature (cm)					**Planform Curvature (cm)**	
Min	-781	-85	**-230**	246	**Min**	**-121**
Max	153	767	**269**	221	**Max**	**138**
Mean	0.0300	0.690	**0.370**	0.247	**Mean**	**1.75**
Std. Deviation	20.4	51.0	**26.0**	11.2	**Std. Deviation**	**23.9**

Table 5. Axial center of channel (black line in Figure 3) wave crest change between 2016 surveys. Positive numbers indicate change in the flood direction (into Tampa Bay) and negative numbers indicate change in the ebb direction (out of Tampa Bay). Green boxes indicate change in the positive direction, and red boxes indicate change in the negative direction. Note that wave crest packages 4a, 4b, and 4c split and join each other (indicated with red numbers).

Wave Crest Package	Distance along profile (m) 05/11/2016 to 06/27/2016	Distance along profile (m) 06/27/2016 to 07/17/2016	Distance along profile (m) 07/17/2016 to 09/14/2016
1	0.20	0.42	-1.3
2	1.2	0.46	-0.43
3	0.43	0.91	-0.57
4a	0.88	0.36	-1.1
4b	0.41	1.4	0.52
4c	0.46	0.65	-1.1
5	0.71	0.20	-0.48
6	1.1	0.40	-0.38
7	1.1	0.72	-0.54
8	0.56	0.28	-0.87
9	0.92	-0.05	-0.34
10	0.64	0.75	-1.0
11	0.95	0.40	-0.76
12	1.2	0.65	0.4
13	1.3	0.13	-0.26
14	1.4	0.19	-0.58

*flood direction (towards the north east) is positive

Table 6. Sediment sample properties, including location, carbonate fraction, and grain size. Colors and data within A correspond to Figures 4 and 9, and colors and data within B correspond to Figure 5.

A	Sample Site 1	Sample Site 2	Sample Site 3	Sample Site 4
Latitude	27.61861	27.620186	27.6215	27.623444
Longitude	-82.65805	-82.655013	-82.653194	-82.65047
Depth (m)	17.6	21.7	16.8	17.1
% Carbonate	38.19	25.95	87.65	68.13
% Other	61.81	74.04	12.35	31.87
Very Fine Gravel and Larger	11.21	30.02	34.46	13.78
Very Coarse Sand	3.70	3.55	21.06	21.14
Coarse sand	10.03	3.55	34.40	27.27
Medium Sand	43.42	13.01	10.77	22.53
Fine Sand	30.19	44.95	1.33	13.92
Very Fine sand	1.15	3.55	0.00	0.52
Silt	0.09	0.15	0.09	0.13
Clay	0.05	0.00	0.00	0.03

B		Sample Site 1		Sample Site 2		Sample Site 3		Sample Site 4	
Grain Size (Wentworth Scale)	**Grain Size (phi)**	**Mean % Volume**	**Std. Dev.**	**Mean % Volume**	**Std. Dev.**	**Mean % Volume**	**Std. Dev.**	**Mean % Volume**	**Std. Dev.**
Very Fine Gravel and Larger	**-1.5**	8.84	3.42	28.60	0.00	28.19	63.84	8.98	2.00
	-1	2.37	1.85	1.42	0.00	6.27	58.44	4.81	2.36
Very Coarse Sand	**-0.5**	1.07	1.82	0.00	0.00	2.91	5.81	8.53	15.71
	0	2.63	3.19	3.55	0.00	18.15	14.61	12.62	16.82
Coarse sand	**0.5**	4.23	5.33	1.18	0.00	11.19	15.65	11.30	11.82
	1	5.79	4.11	2.37	0.00	23.21	13.17	15.98	10.48
Medium Sand	**1.5**	11.02	1.92	3.55	0.00	7.90	4.56	9.49	3.21
	2	32.40	5.32	9.46	0.00	2.87	2.72	13.04	6.19
Fine Sand	**2.5**	27.24	6.80	28.98	0.00	0.16	0.33	11.32	10.81
	3	2.95	0.91	15.97	0.00	1.17	0.19	2.60	1.80
Very Fine sand	**3.5**	0.82	0.77	2.37	0.00	0.00	0.00	0.34	0.68
	4	0.34	0.75	1.18	0.00	0.00	0.00	0.18	0.35
Silt	**8**	0.09	0.00	0.15	0.00	0.09	0.00	0.13	0.00
Clay	**12**	0.05	0.00	0.00	0.00	0.00	0.00	0.03	0.00

*Error for pipette analysis is 1%, and settling tube errors are +/- 0.4 phi

FIGURES

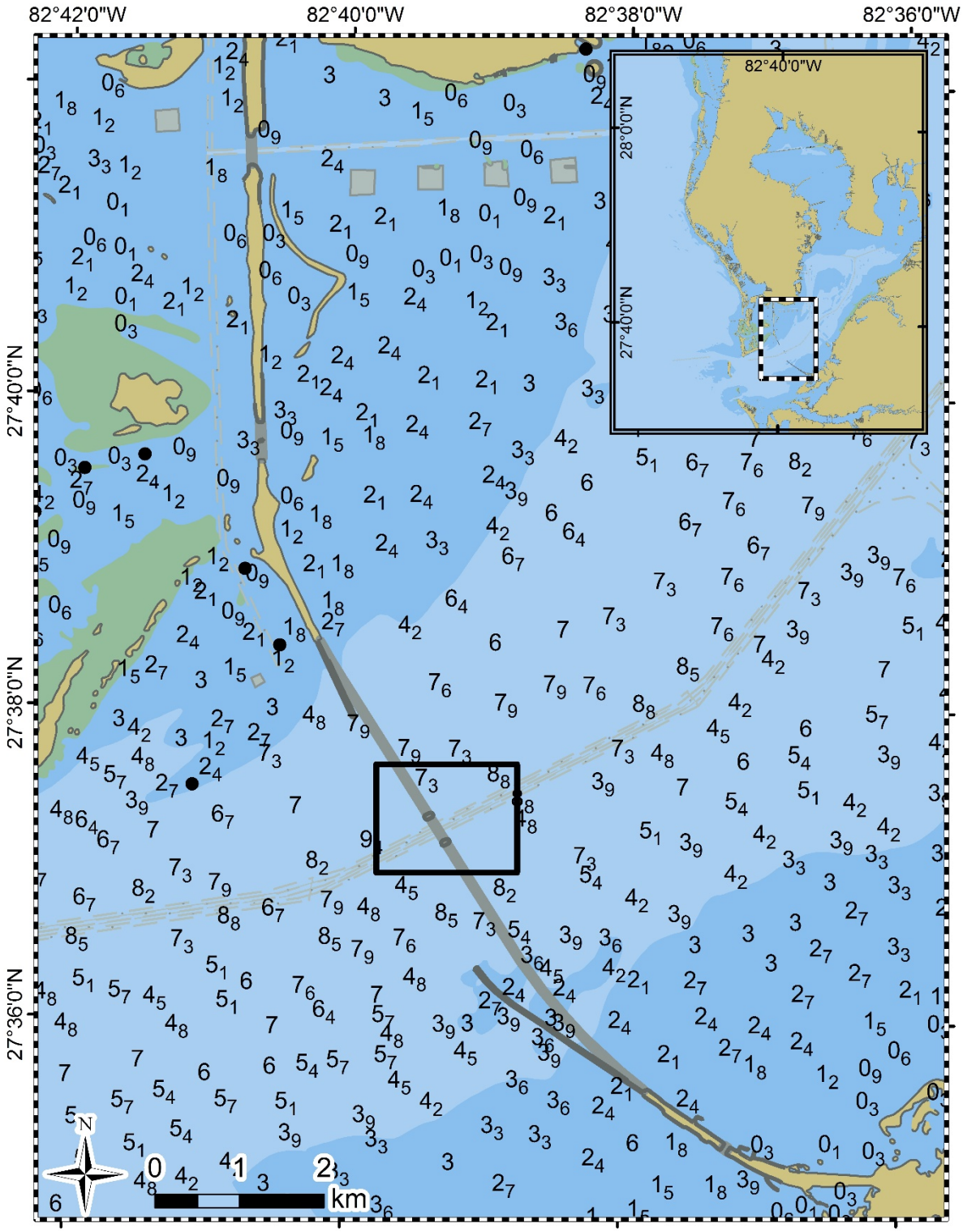

Figure 1. Area of interest near the mouth of Tampa Bay. Dotted-line box within inset matches frame of main map. Black box marks area shown in Figures 3, 4, 8, 9 and 10. Land is beige, tidal areas are green, and water is blue. Bridge structure is shown in dark gray, and channel is marked in light gray. Soundings are shown in meters.

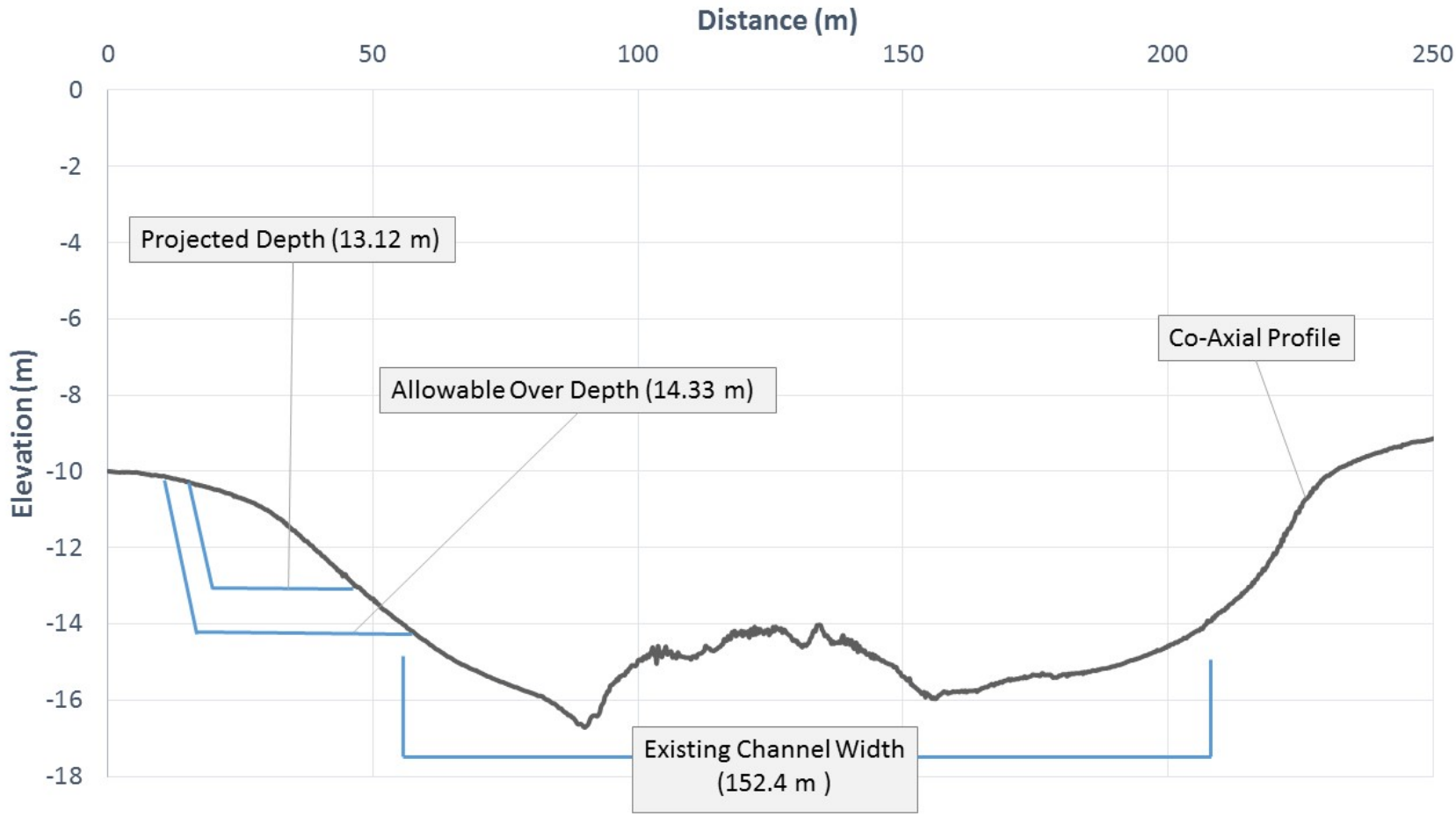

Figure 2. Plans for 30 m channel-widening beneath the Skyway Bridge, depicted on a representative co-axial profile of the shipping channel. Elevation is relative to MLLW.

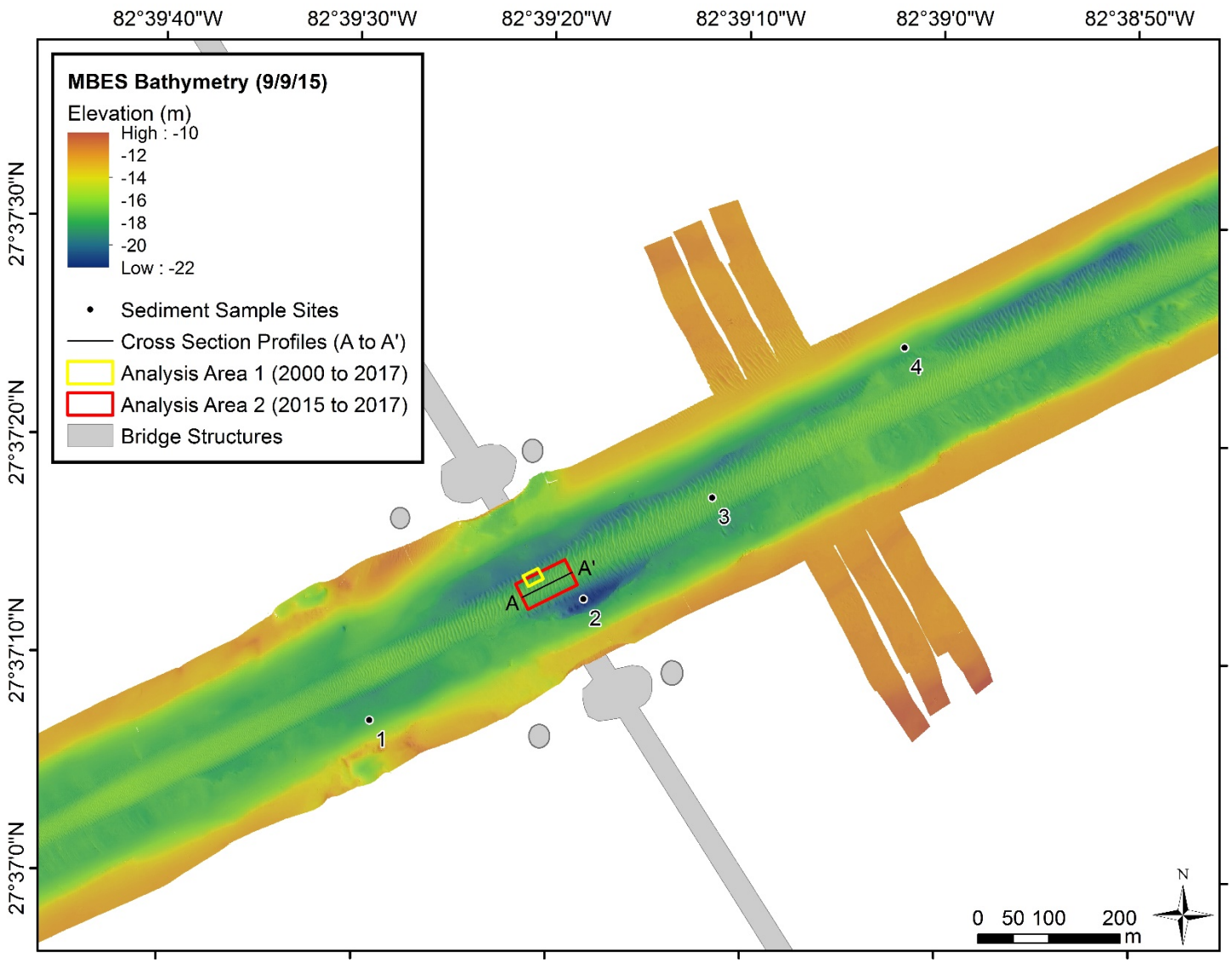

Figure 3. Study areas including September 9, 2015 MBES bathymetry, sediment sample sites, bathymetry analysis areas, and cross-section location from A to A'. Frame of figure matches location of black box in Figure 1. All dates are formatted month/day/year.

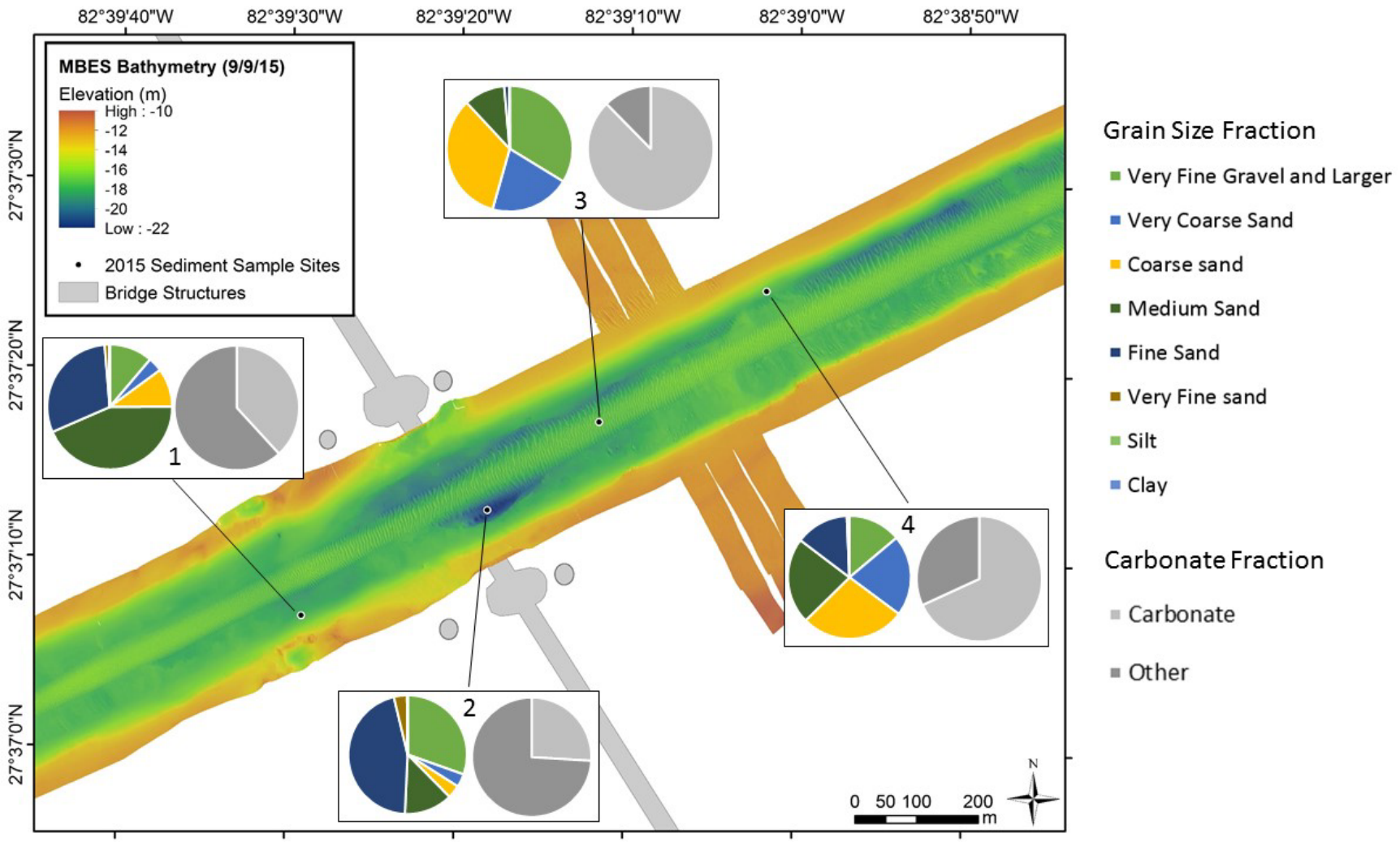

Figure 4. Grain size fraction and carbonate fraction pie charts for each sediment sample site, shown with September 9, 2015 MBES bathymetry. Frame of figure matches location of black box in Figure 1. All dates are formatted month/day/year.

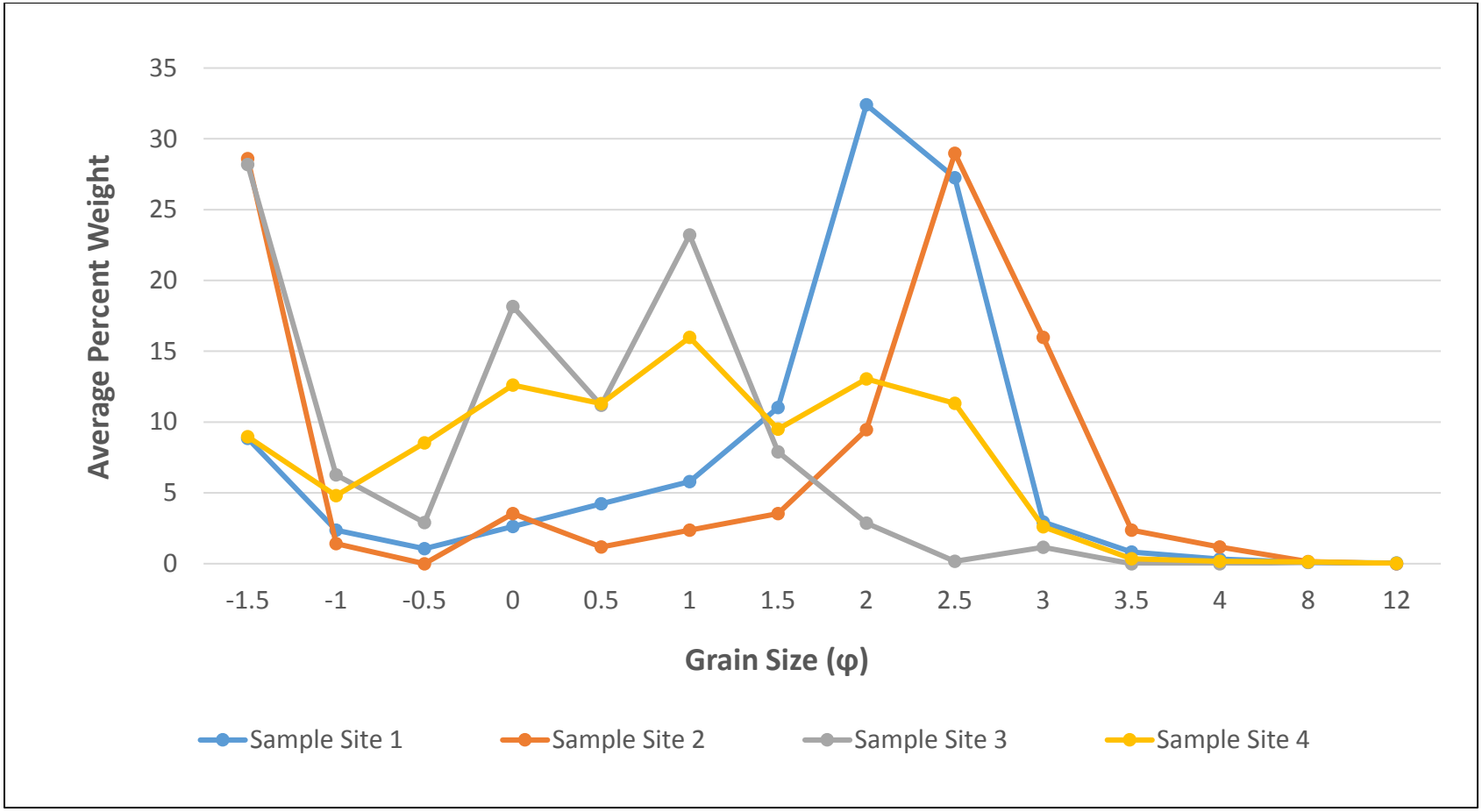

Figure 5. Grain size (x-axis) vs. proportion of sample (y-axis) for each sediment sample site. Locations of sediment samples shown in Figure 3. Note the comparatively larger grain sizes found in the third sample.

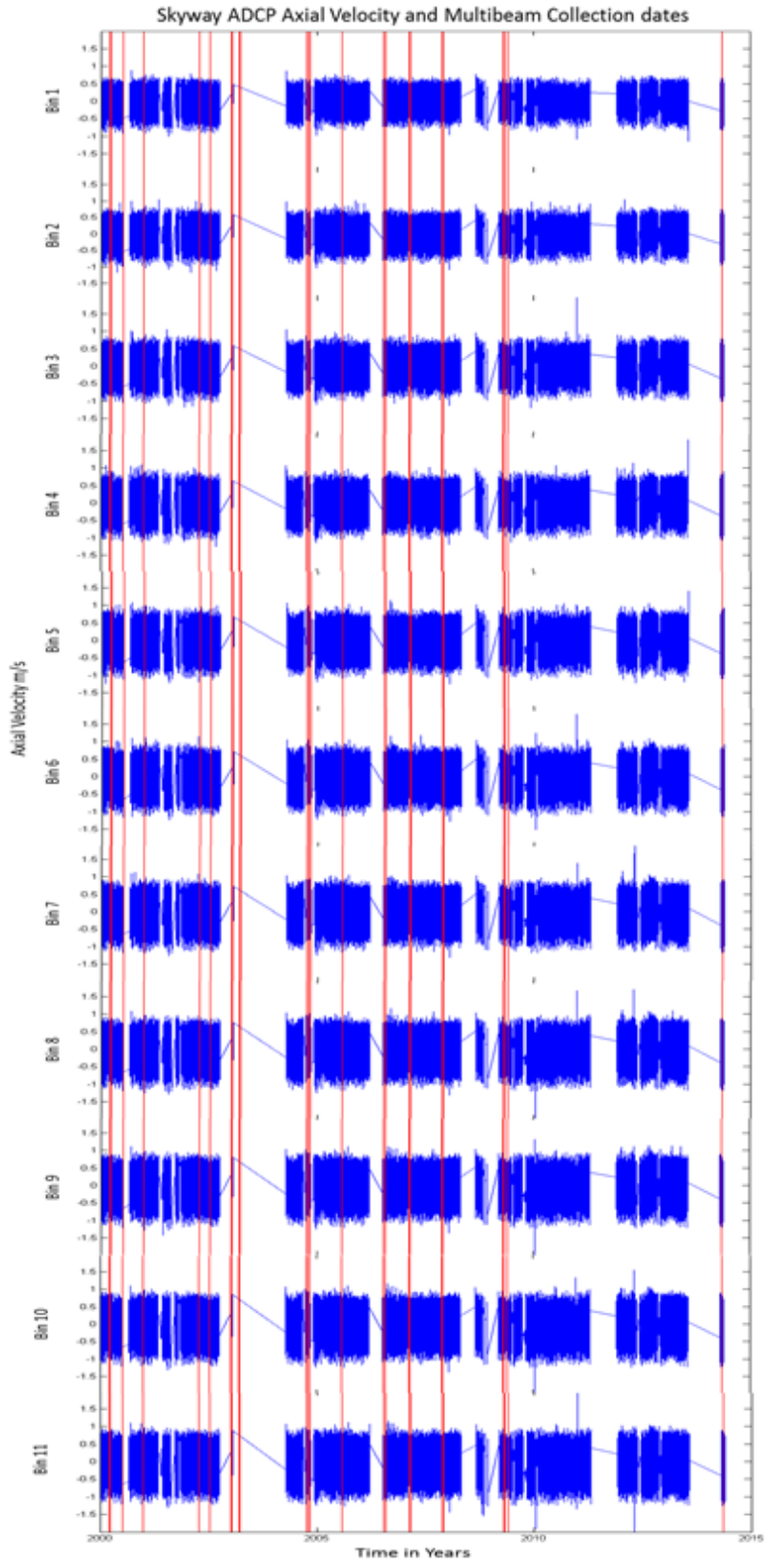

Figure 6. ADCP data from 2000 to 2015 including all bins, where bin 1 is deepest and Bin 11 is shallowest. Red lines indicate MBES survey dates during this time period.

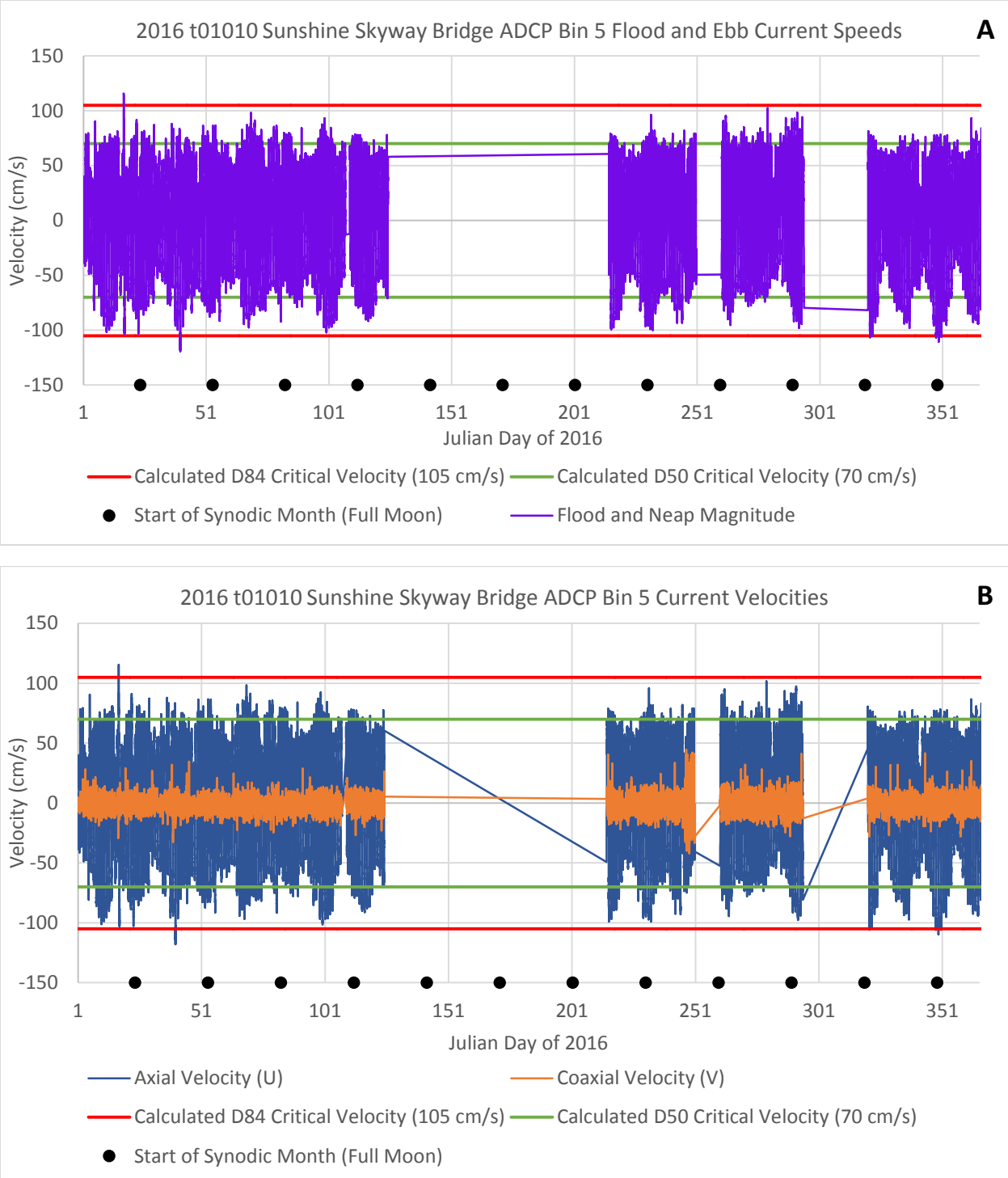

Figure 7. Flood and ebb current speeds (A) and axial and coaxial current velocities (B) from Bin 5 of the t01010 Sunshine Skyway Bridge ADCP record, shown with critical velocities and full moon dates.

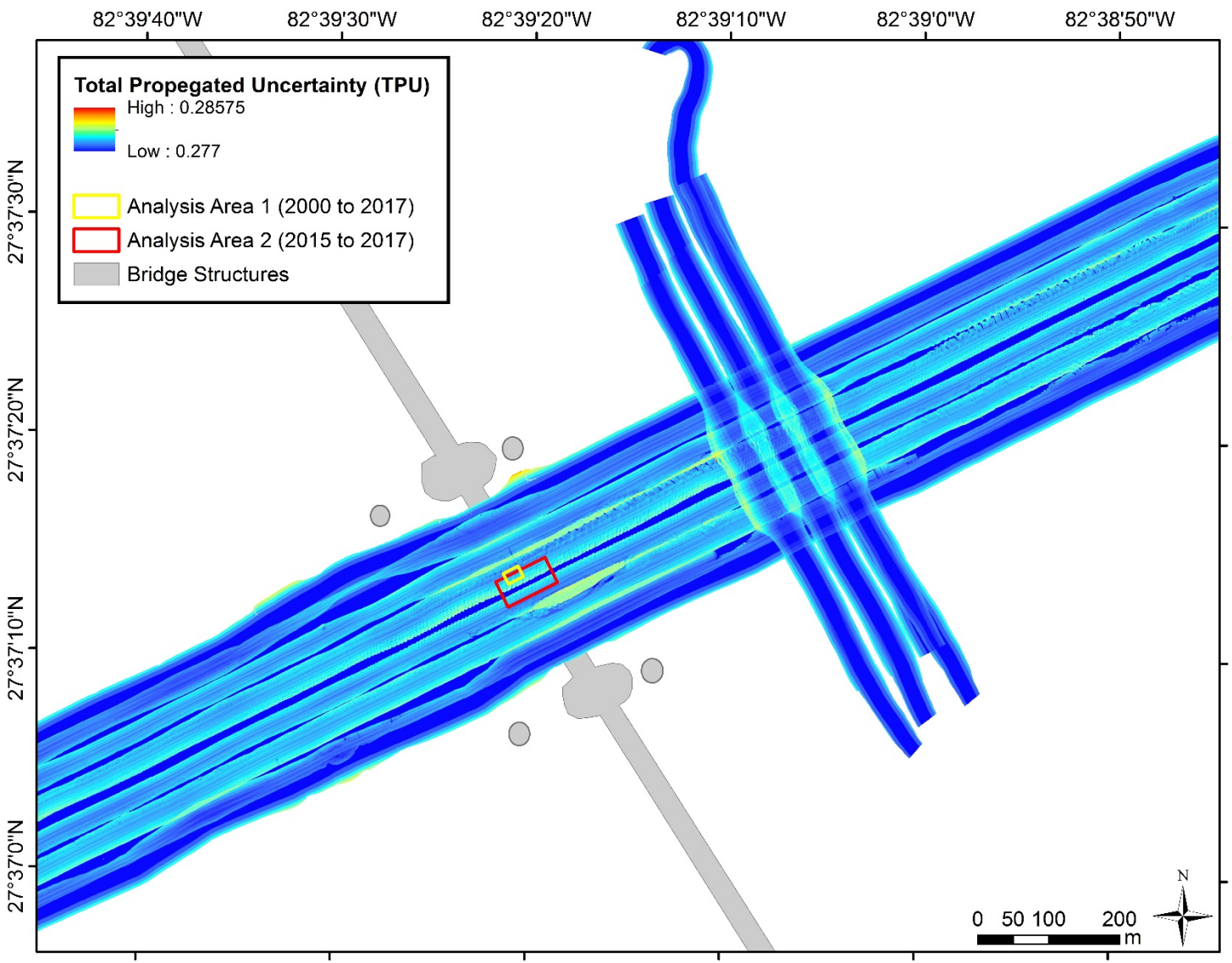

Figure 8. Total propagated uncertainty (TPU) of MBES bathymetry data collected on September 9, 2015. Note small range of TPU (0.277–0.286) throughout the survey area. Frame of figure matches location of black box in Figure 1. All dates are formatted month/day/year.

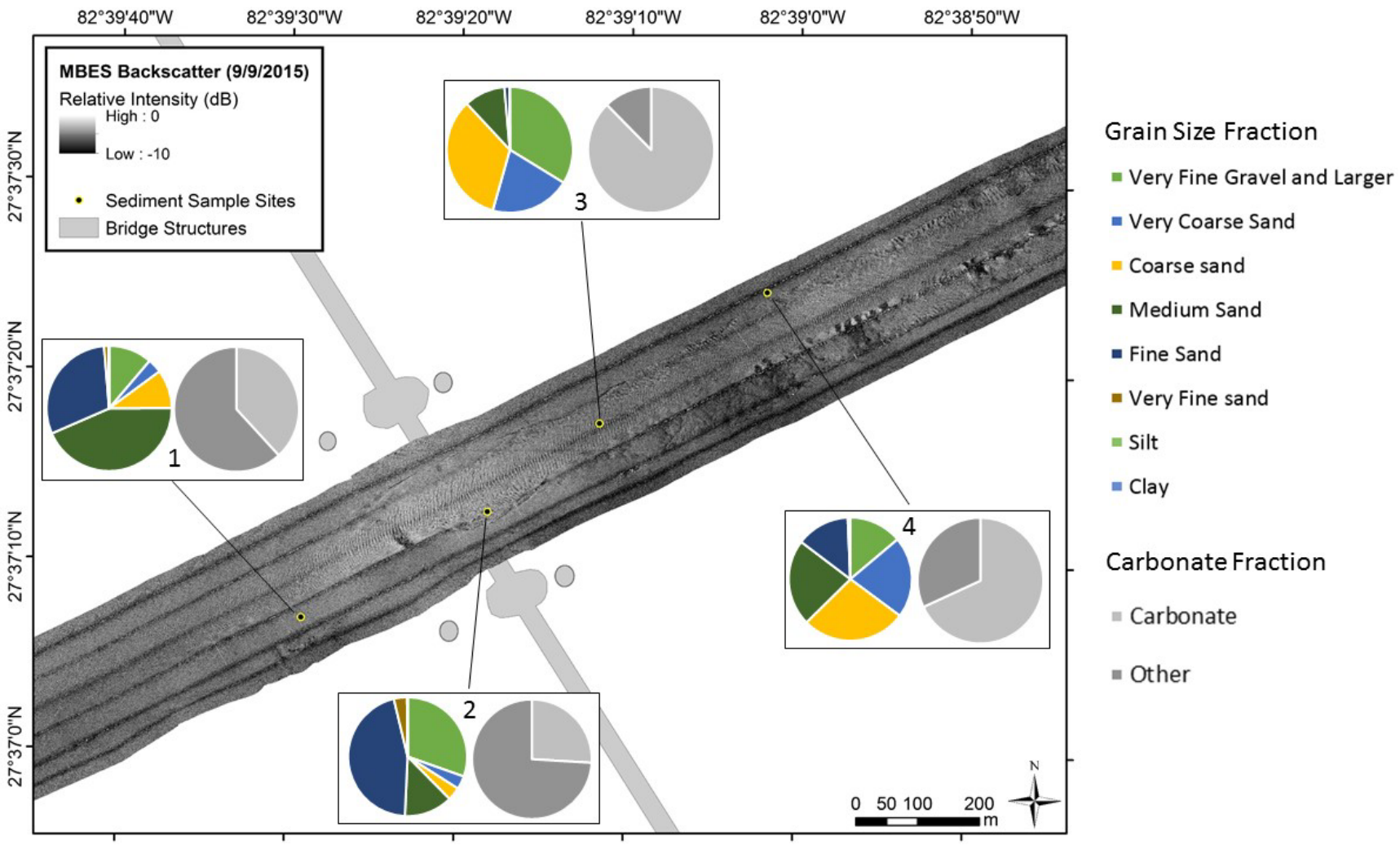

Figure 9. Backscatter intensity mosaic derived from 400 kHz multibeam time-series data collected on September 9, 2015, with locations and analysis of sediment samples collected on the same day. Frame of figure matches location of black box in Figure 1. All dates are formatted month/day/year.

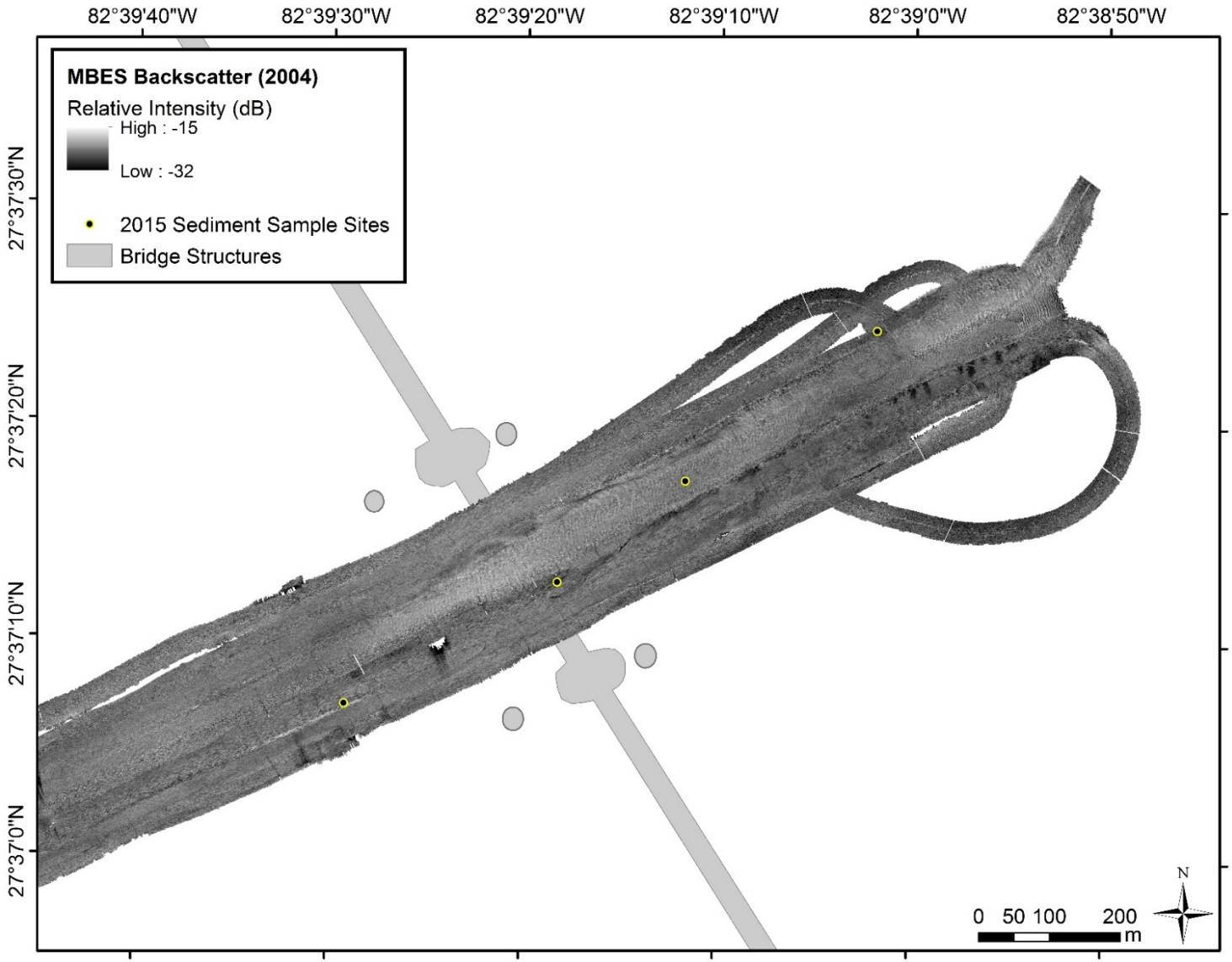

Figure 10. Backscatter intensity mosaic derived from 300 kHz multibeam time-series data collected in 2004, with locations of sediment samples collected 11 years later in 2015. Frame of figure matches location of black box in Figure 1.

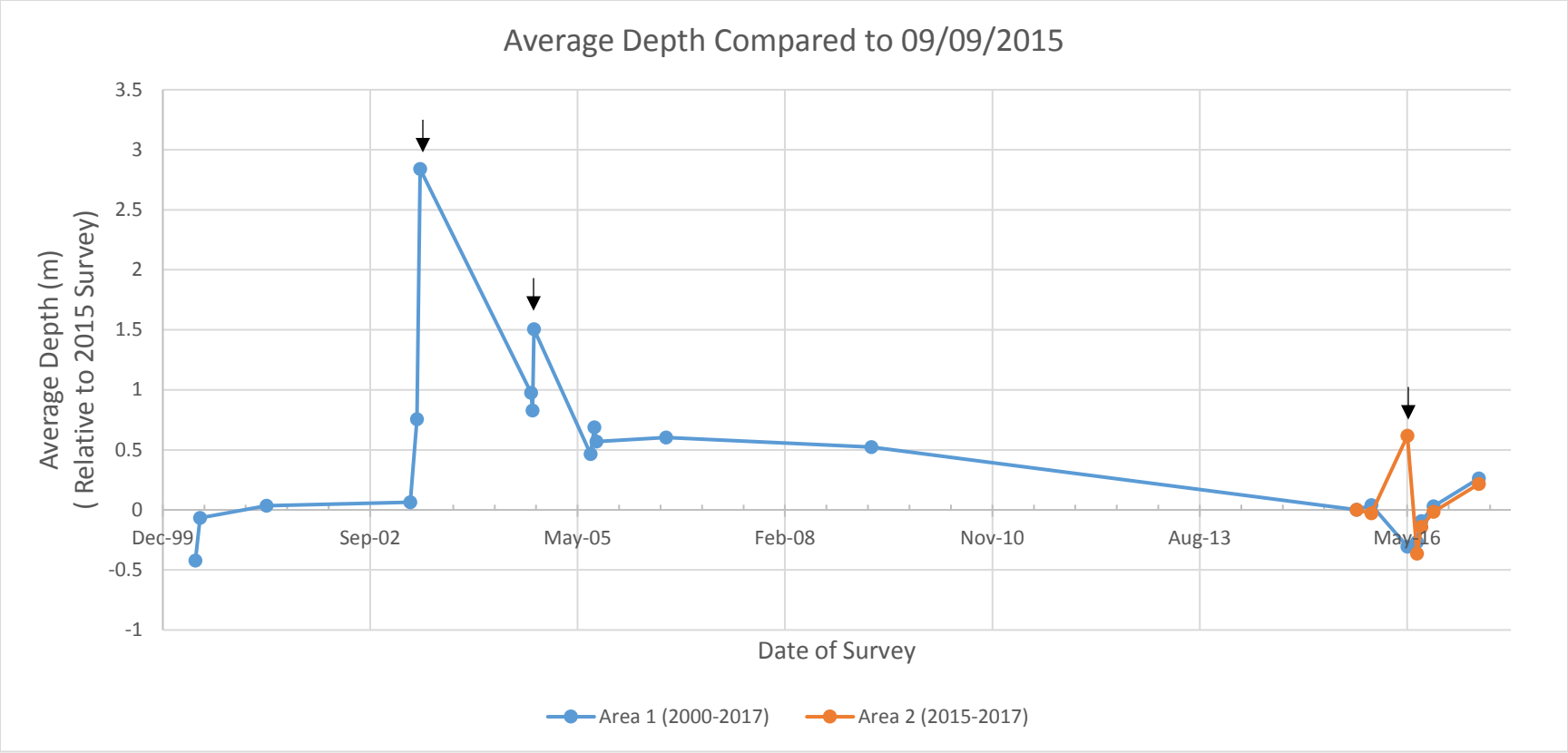

Figure 11. Average depth in Analysis Areas 1 and 2 with reference to the September 9, 2015 survey as zero. Data points indicated with arrows are highly suspect. Uncertainty in absolute depth is high due to the nature of transit multibeam data and factors that could not be accounted for.

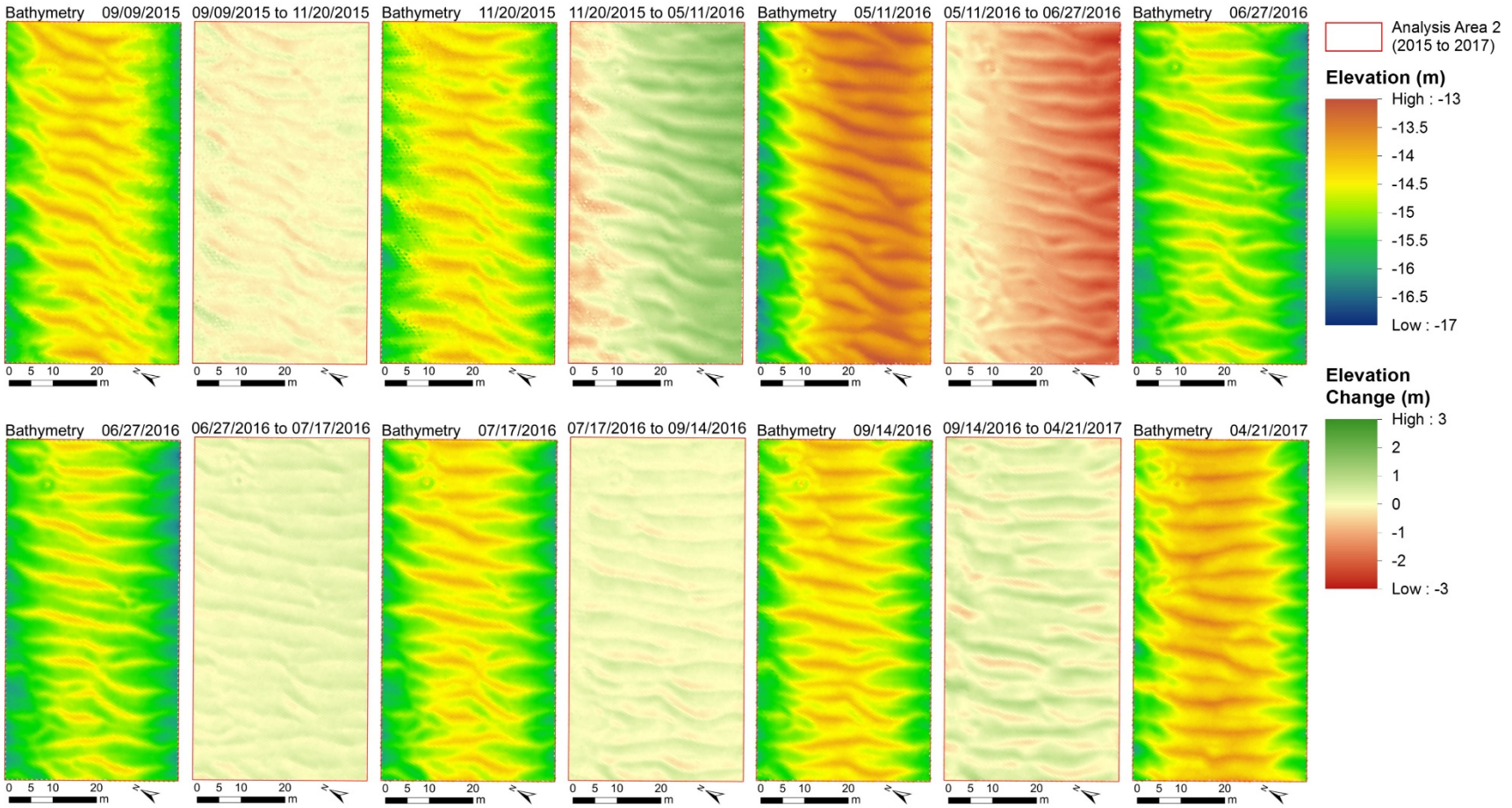

Figure 12. Bathymetry from seven consecutive MBES surveys, with surface change calculations between each survey. Red box corresponds to red box in Figure 3. Elevation legend applies to all panels labeled "Bathymetry", Elevation Change legend applies to all panels labeled with date ranges. All dates are formatted month/day/year. Note that the last survey on the top row is repeated at the beginning of the bottom row.

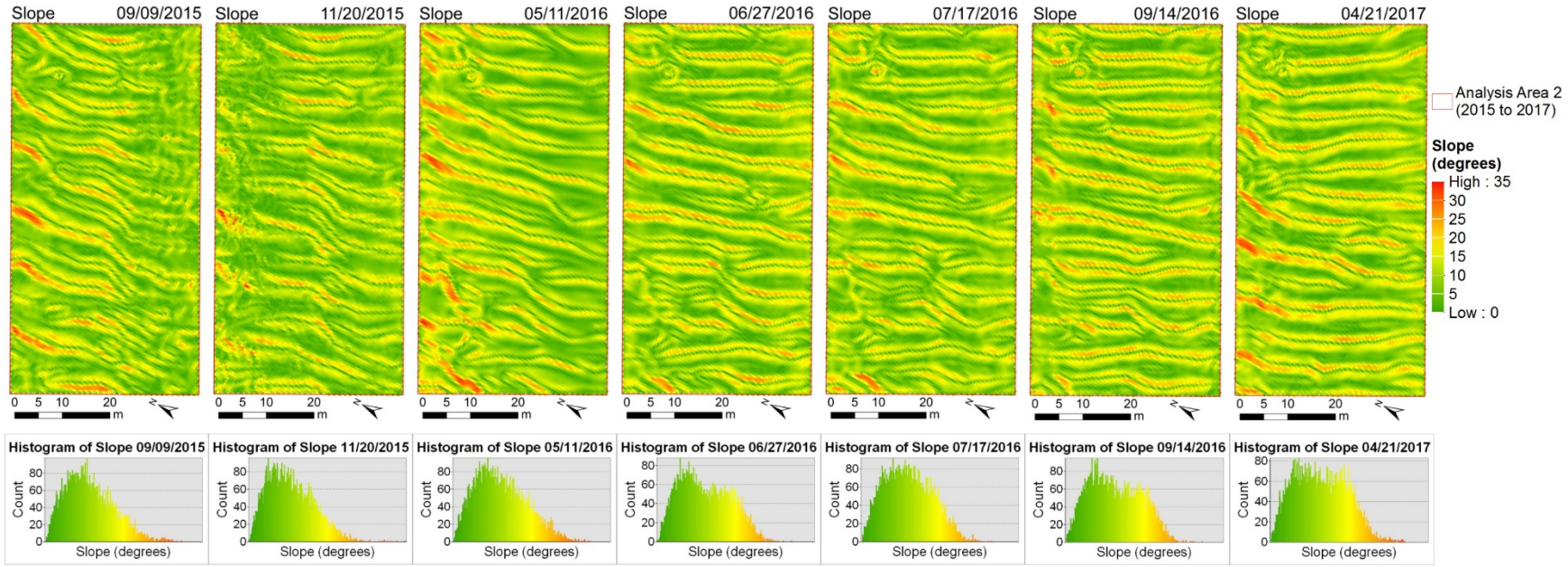

Figure 13. Slope calculated from MBES bathymetry in Analysis Area 2, with corresponding histogram beneath each map panel. Red box corresponds to the red box in Figure 3. Slope color in legend applies to all map panels and all histograms. All dates are formatted month/day/year.

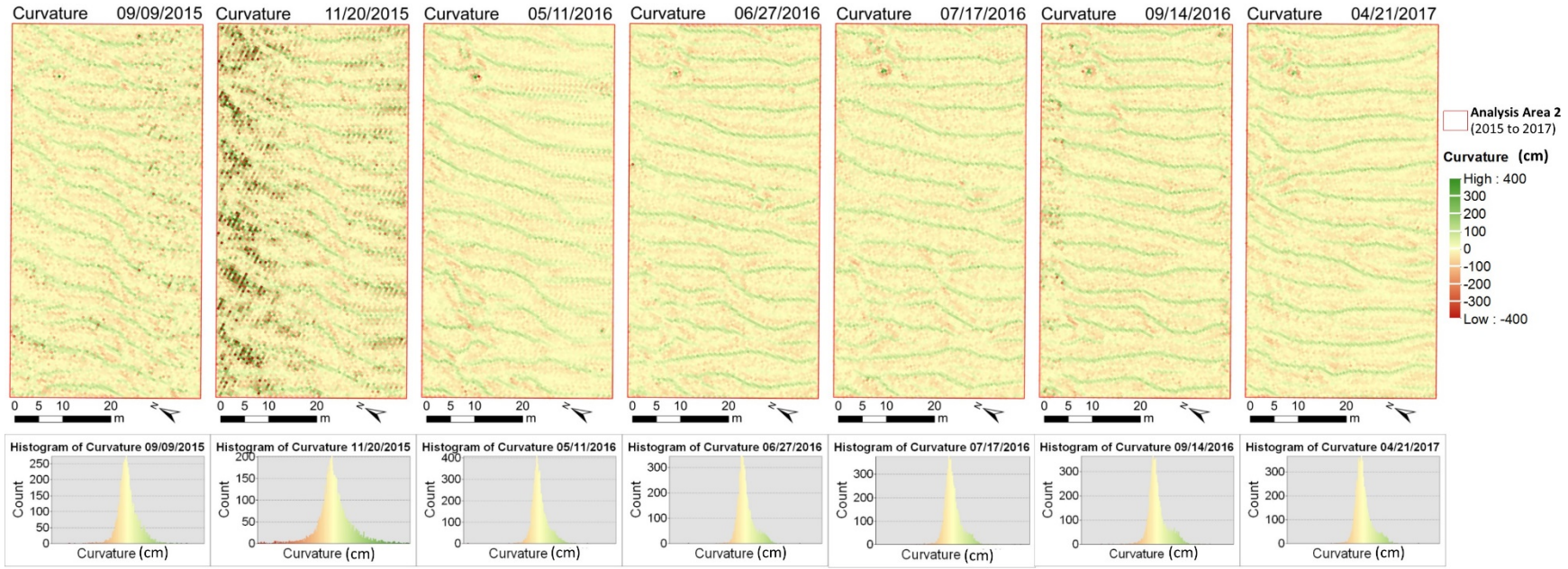

Figure 14. Curvature, derived as slope of slope calculated from MBES bathymetry in Analysis Area 2, with corresponding histogram beneath each map panel. Red box corresponds to the red box in Figure 3. Curvature color in legend applies to all map panels and all histograms. All dates are formatted month/day/year.

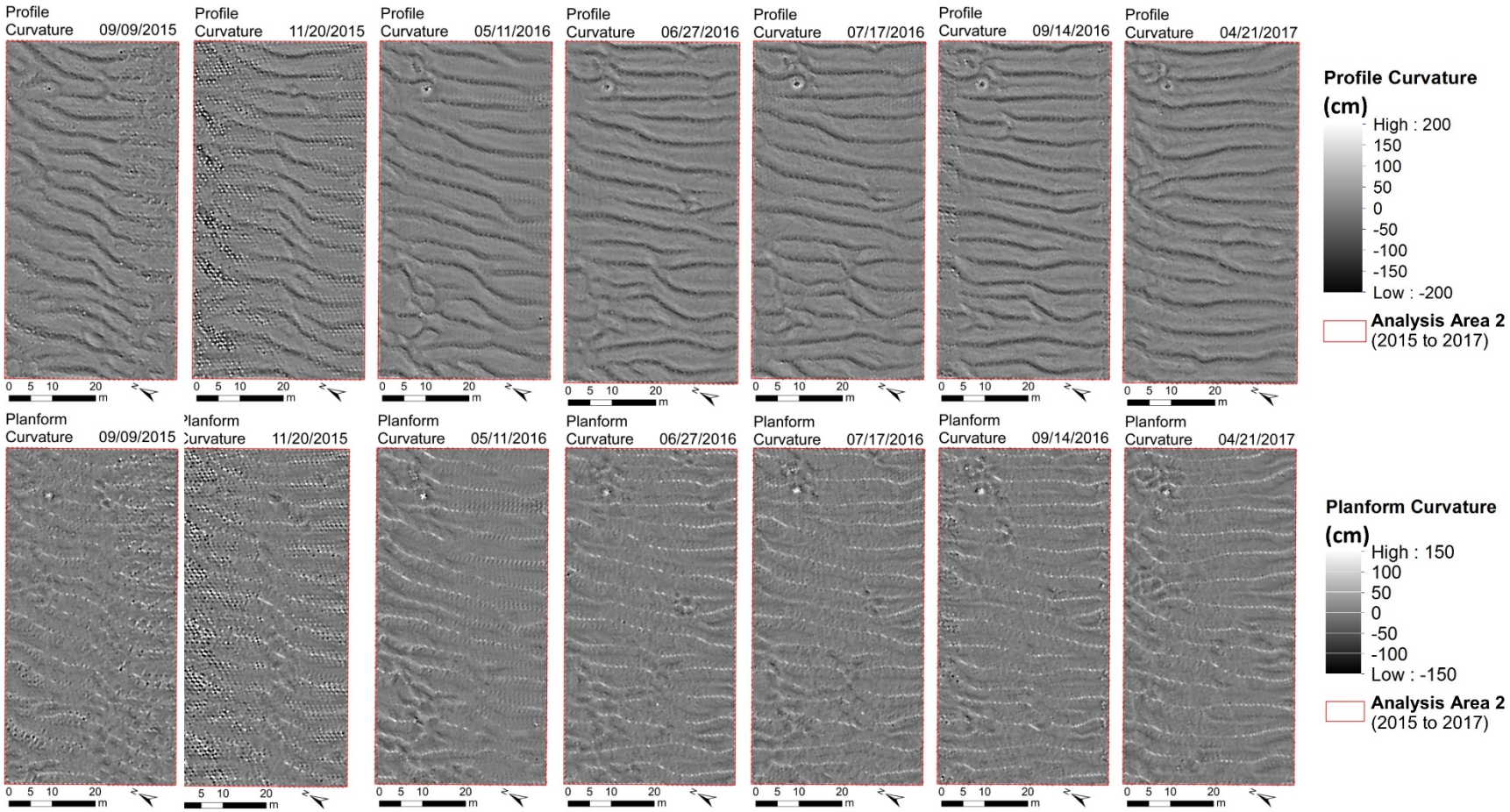

Figure 15. Profile curvature (top), derived as slope of slope along-slope and planform curvature (bottom) derived as slope of slope across-slope, calculated from MBES bathymetry in Analysis Area 2. Red box corresponds to the red box in Figure 3. Profile curvature color in legend applies to all map panels in the top row and planform curvature color in legend applies to all map panels in the bottom row. All dates are formatted month/day/year.

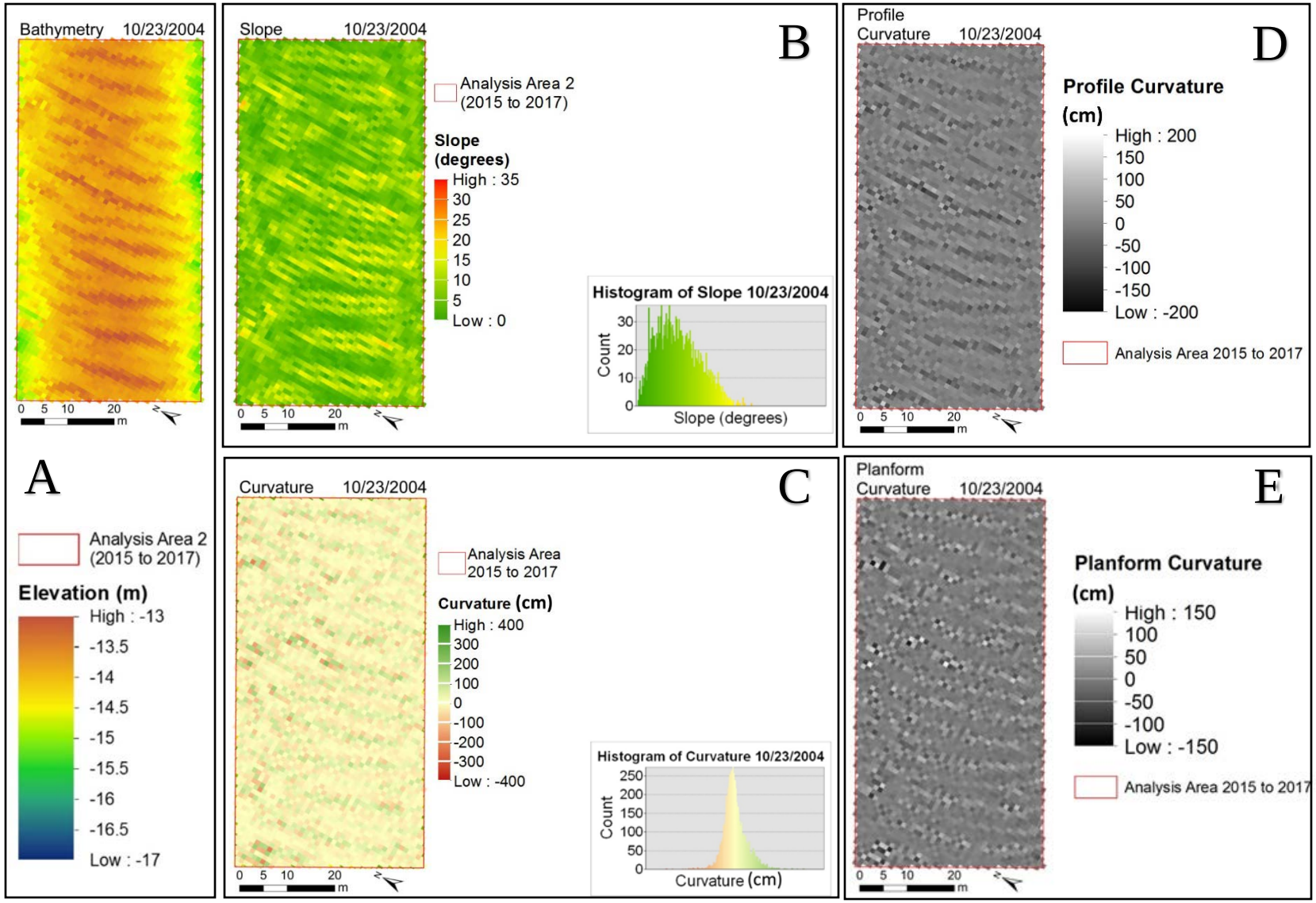

Figure 16. Bathymetry and bathymetry-derived characteristics of Analysis Area 2 in 2004, including a) bathymetry, b) slope, c) curvature, d) profile curvature, and e) planform curvature. Red box in all panels corresponds to red box in Figure 3. All dates are formatted month/day/year.

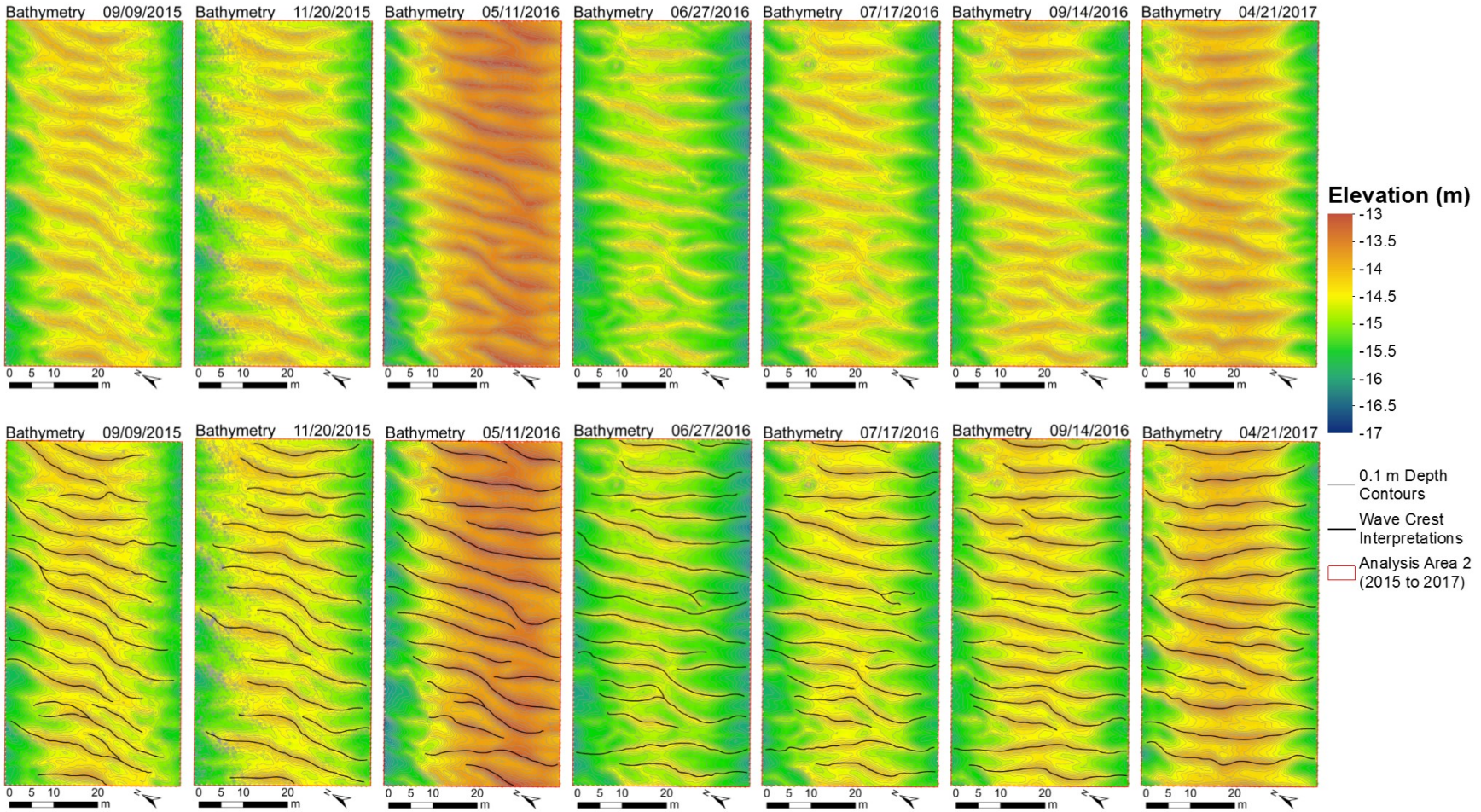

Figure 17. Bathymetry for surveys from 2015–2017 shown with 0.1 m depth contours used for wave crest interpretations, both without (top panels) and with (bottom panels) wave crest interpretations shown in bold black lines. Elevation color ramp applies to all map panels. Red box in all map panels corresponds to the red box in Figure 3. All dates are formatted month/day/year.

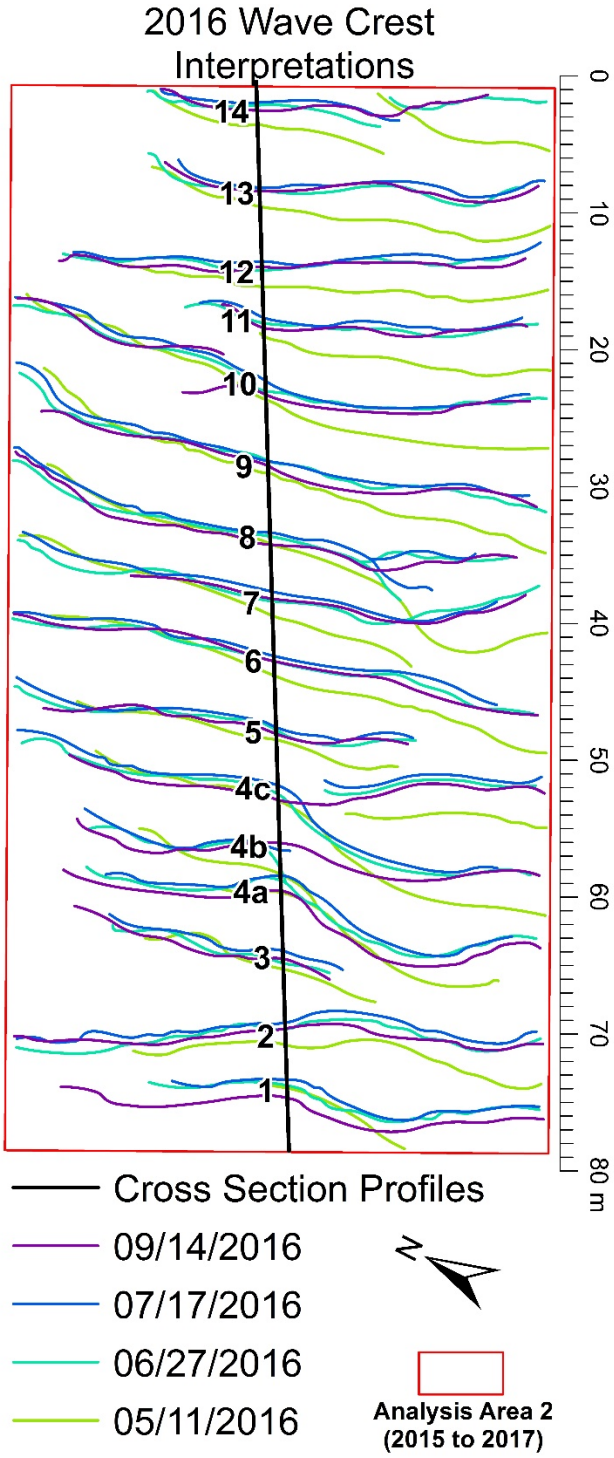

Figure 18. Wave crest interpretations from 2016 surveys. Each survey date is displayed in a different color. Wave crest packages, which are likely the same bed form from survey to survey, are numbered from southwest to northeast. Black line indicates location of cross section profiles. Movement of bedforms from survey to survey was measured along the cross section profile line. Red box corresponds to the red box shown in Figure 3. All dates are formatted month/day/year.

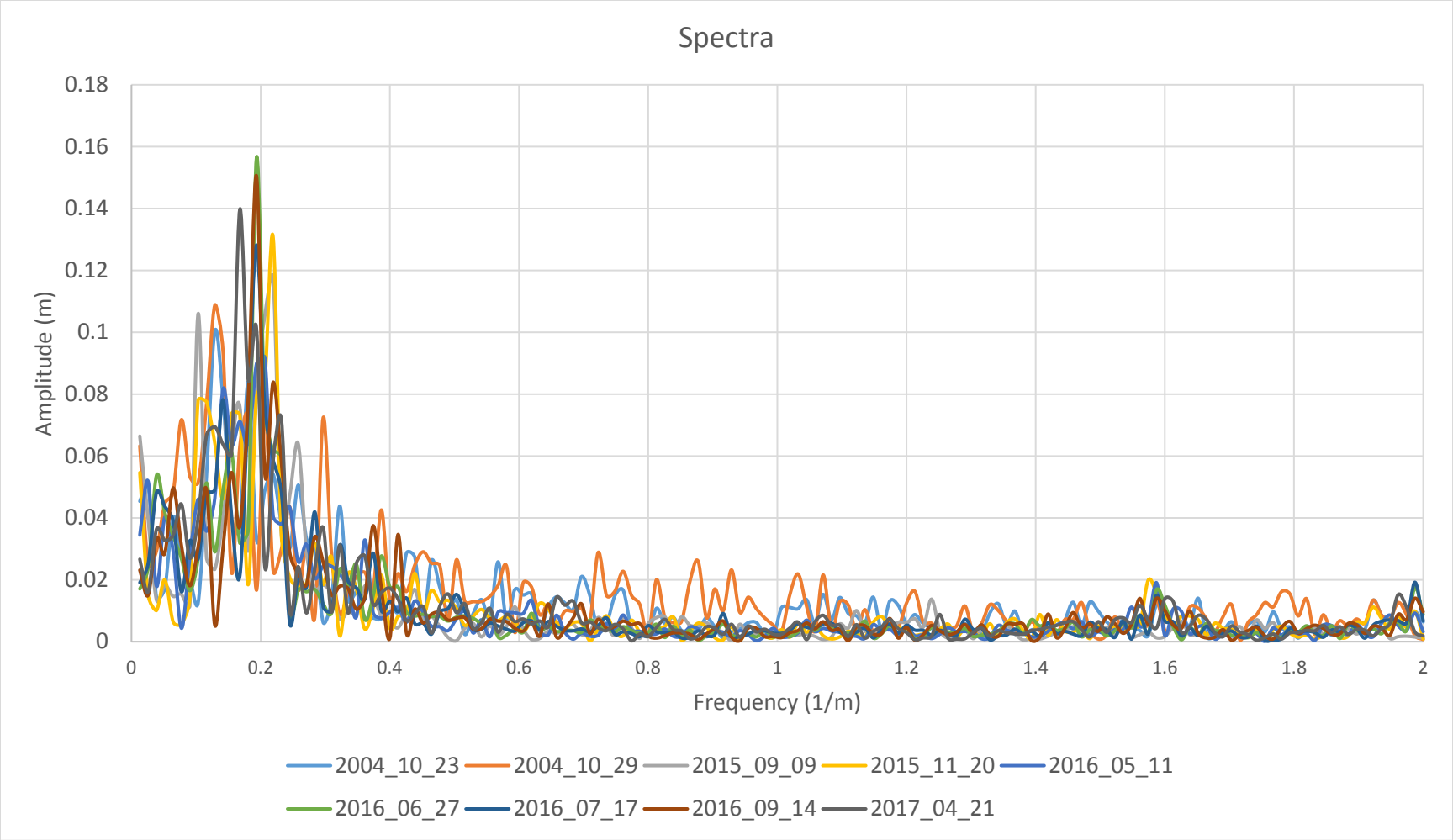

Figure 19. Spectra of detrended sand wave bedforms along axial cross section (black line in Figure 3) resulting from a fast Fourier transform analysis. Spectra of sand wave bedforms from each survey date is shown in a different color.

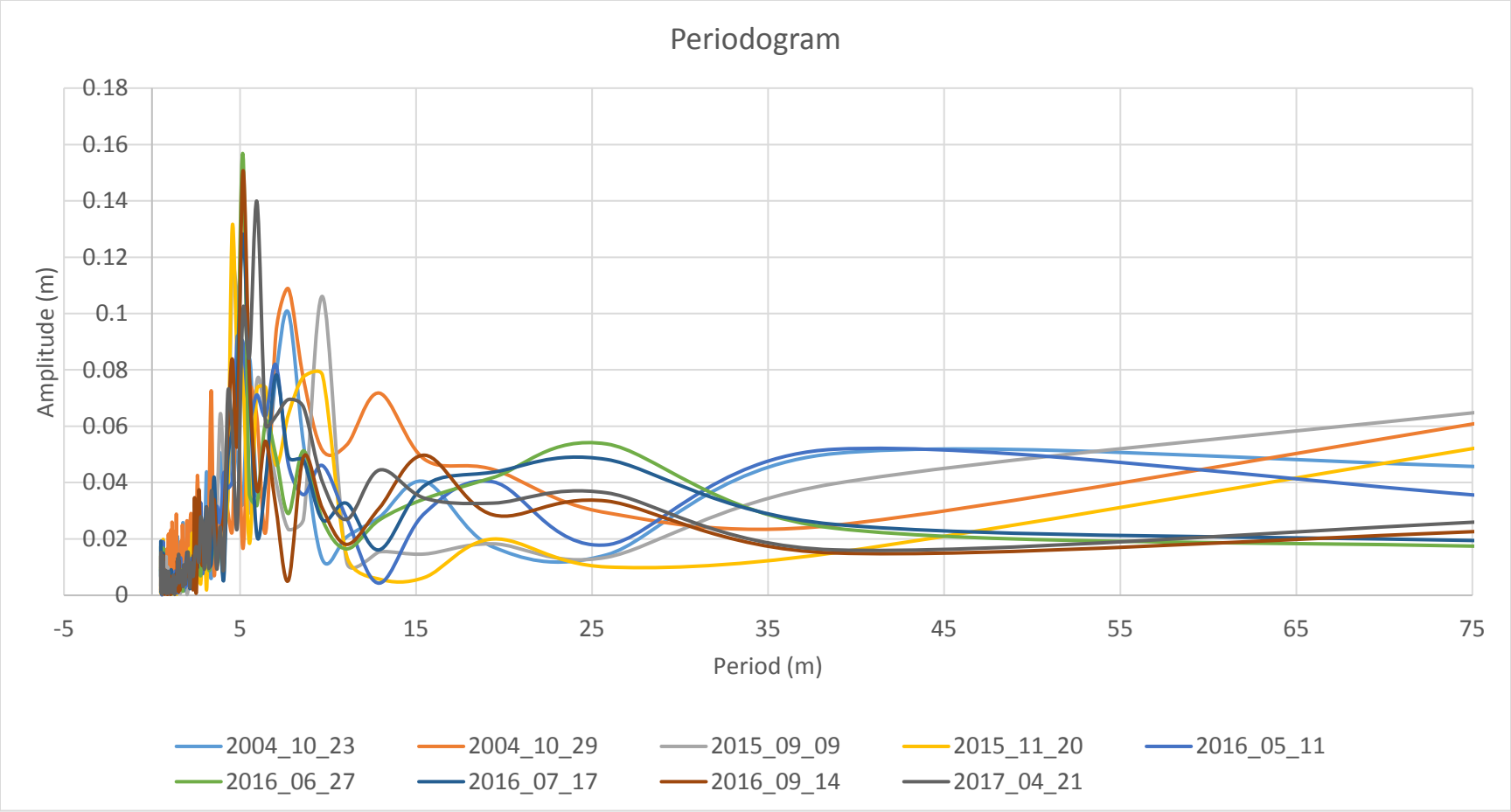

Figure 20. Period (x-axis) compared to amplitude (y-axis) of detrended sand wave bedforms along axial cross section (black line in Figure 3), resulting from a fast Fourier transform analysis. Periodogram of sand wave bedforms from each survey date is shown in a different color.

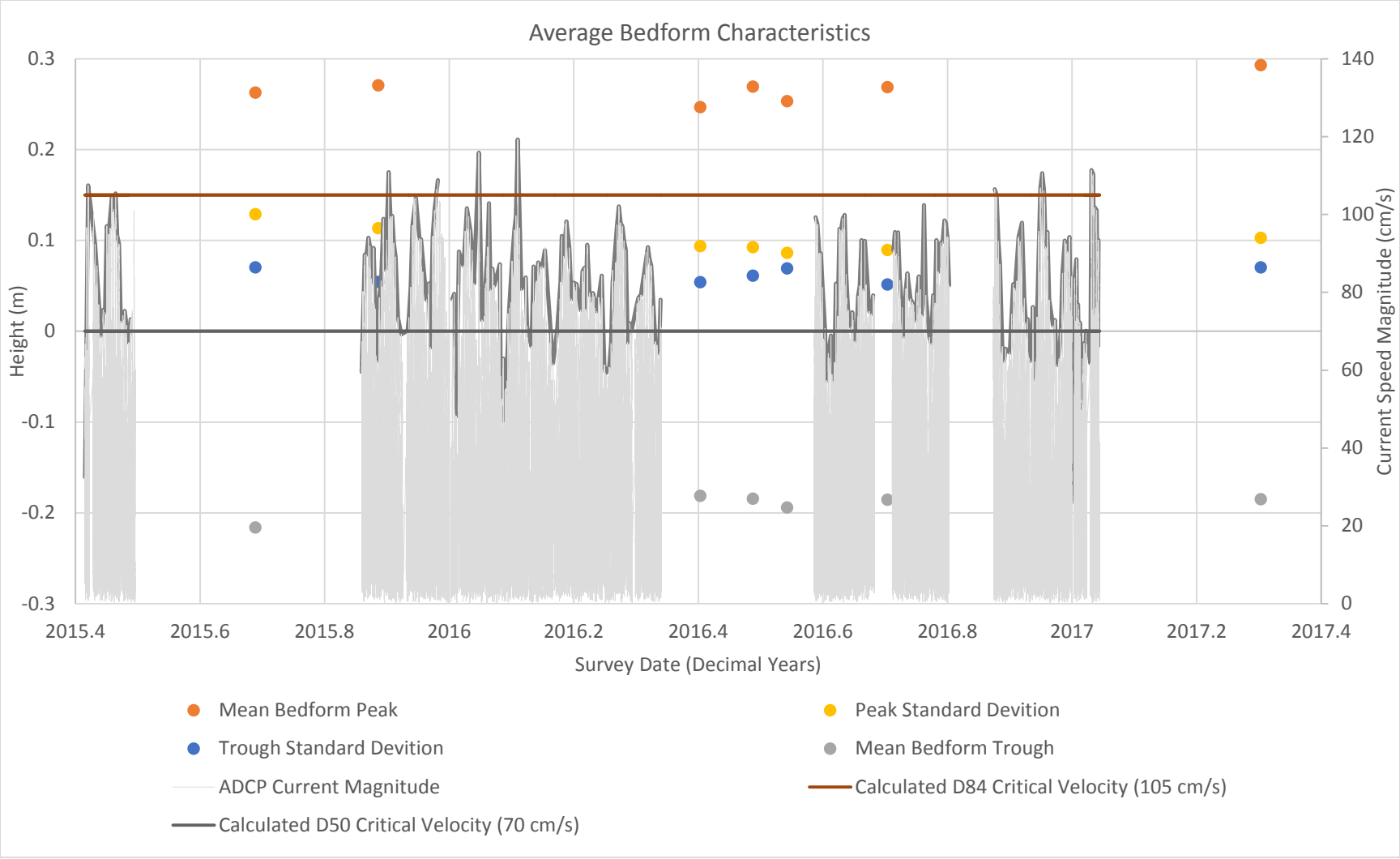

Figure 21. Average bedform characteristics for each survey from 2015 to 2017, shown with ADCP current magnitudes and calculated critical velocities over time.

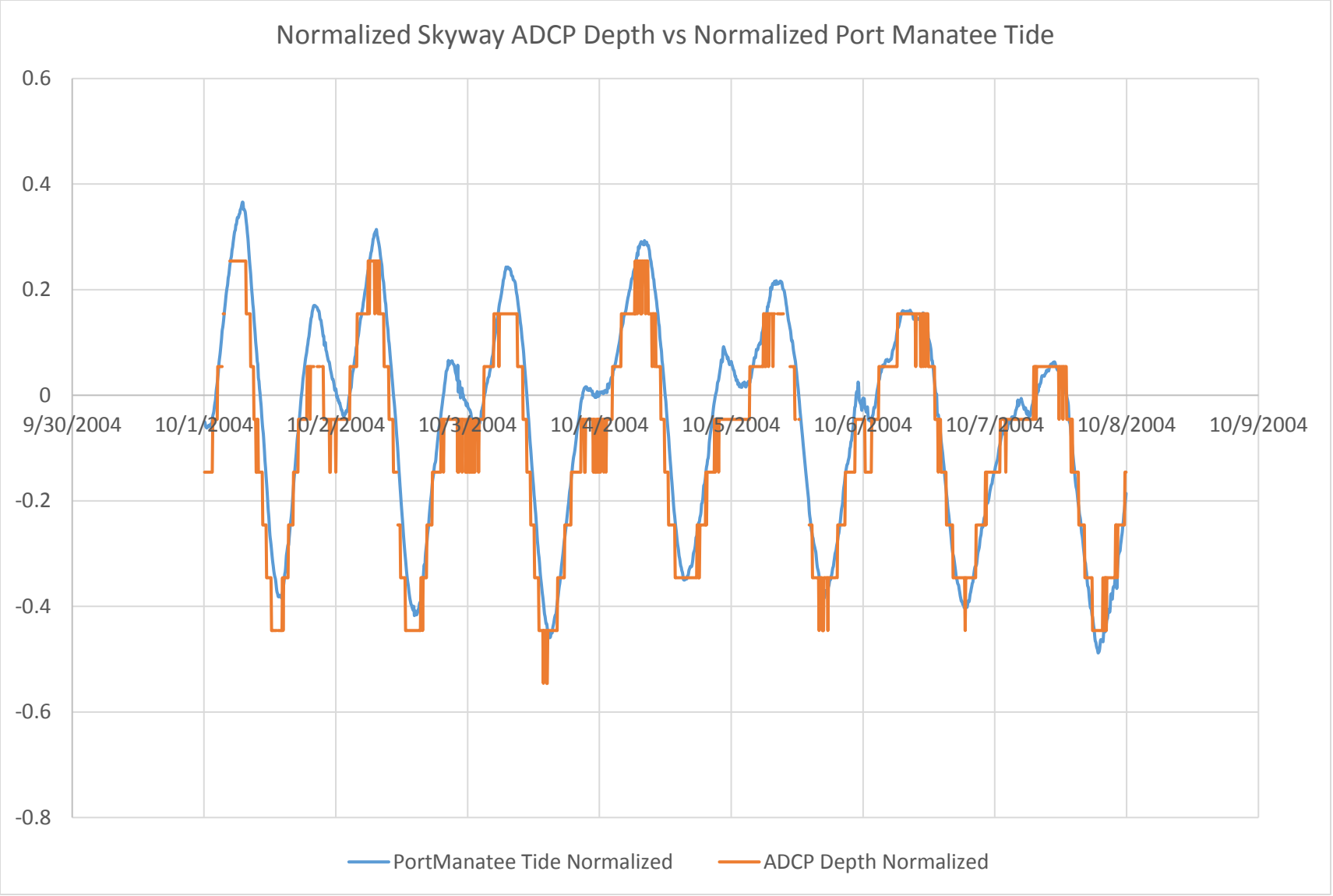

Figure 22. Normalized tide at Port Mantatee tide gauge shown with normalized depth from the ADCP beneath the Sunshine Skyway Bridge from October 1, 2004 to October 7, 2004.